

ChAInGeS: The Chandra Arp Interacting Galaxies Survey

Beverly J. Smith¹, Douglas A. Swartz², Olivia Miller¹, Jacob A. Burleson³, Michael A. Nowak⁴, and Curtis Struck⁵

ABSTRACT

We have conducted a statistical analysis of the ultra-luminous X-ray point sources (ULXs; $L_X \geq 10^{39}$ erg/s) in a sample of galaxies selected from the Arp Atlas of Peculiar Galaxies. We find a possible enhancement of a factor of $\sim 2-4$ in the number of ULXs per blue luminosity for the strongly interacting subset. Such an enhancement would be expected if ULX production is related to star formation, as interacting galaxies tend to have enhanced star formation rates on average. For most of the Arp galaxies in our sample, the total number of ULXs compared to the far-infrared luminosity is consistent with values found earlier for spiral galaxies. This suggests that for these galaxies, ULXs trace recent star formation. However, for the most infrared-luminous galaxies, we find a deficiency of ULXs compared to the infrared luminosity. For these very infrared-luminous galaxies, AGNs may contribute to powering the far-infrared; alternatively, ULXs may be highly obscured in the X-ray in these galaxies and therefore not detected by these Chandra observations. We determined local UV/optical colors within the galaxies in the vicinity of the candidate ULXs using GALEX UV and SDSS optical images. In most cases, the distributions of colors are similar to the global colors of interacting galaxies. However, the $u - g$ and $r - i$ colors at the ULX locations tend to be bluer on average than these global colors, suggesting that ULXs are preferentially found in regions with young stellar populations. In the Arp sample there is a possible enhancement of a factor of $\sim 2 - 5$ in the fraction of galactic nuclei that are X-ray bright compared to more normal spirals.

Subject headings: galaxies: starbursts — galaxies: interactions— galaxies: ultraviolet

1. Introduction

In the dozen years since its launch, the *Chandra* X-ray Observatory has discovered hundreds of ultra-luminous ($\geq 10^{39}$ erg/s) X-ray point sources (ULXs) in external galaxies. Several different scenarios have been suggested to explain these sources, including sub-Eddington in-

termediate mass (100 - 1000 M_\odot) black holes (Colbert & Mushotzky 1999; Portegies Zwart et al. 2004a,b; Freitag, Gürkan, & Rasio 2006) or stellar mass black holes with beamed (King et al. 2001; King 2009) or super-Eddington (Begelman 2002) X-ray emission. In a few cases sensitive high resolution optical images have found late O or early B stars that are the apparent mass donors for the ULXs, suggesting stellar mass black holes (Liu, Bregman, & Seitzer 2002, 2004; Kuntz et al. 2005; Ptak et al. 2006; Terashima, Inoue, & Wilson 2006; Roberts, Levan, & Goad 2008; Grisé et al. 2008; Tao et al. 2011). In other cases, emission nebulae have been found that are apparently associated with the ULX (Pakull & Mirioni 2003; Pakull, Grisé, & Motch 2006). However, in most cases a discrete optical counterpart to the ULX is not found.

¹Department of Physics and Astronomy, East Tennessee State University, Johnson City TN 37614; smithbj@etsu.edu; millero@goldmail.etsu.edu

²University Space Research Association, NASA Marshall Space Flight Center, VP 62, Huntsville AL, Douglas.A.Swartz@nasa.gov

³University of Alabama Huntsville AL 35805; jab0039@uah.edu

⁴MIT-CXC, mnowak@space.mit.edu

⁵Department of Physics and Astronomy, Iowa State University, Ames IA 50011; curt@iastate.edu

Statistical studies of the environments of ULXs provide additional clues to their nature. The number of ULXs in spiral galaxies has been found to be correlated with the galaxy’s global star formation rate, suggesting that they are mostly high mass X-ray binaries (HMXBs) (Swartz et al. 2004, 2011; Liu, Bregman, & Irwin 2006). This is consistent with studies that show good correlations of the star formation rate of a galaxy with its global hard X-ray luminosity (Ranalli, Comastri, & Setti 2003; Persic & Rephaeli 2007) and with the number of HMXBs (Grimm et al. 2003; Mineo et al. 2012). For ellipticals and low mass spirals, the ULX frequency seems to be better correlated with the stellar mass, and the ULX luminosities tend to be lower, suggesting that these sources may be the high luminosity end of the low mass X-ray binary population (LMXBs) (Swartz et al. 2004). In general, LMXBs appear to be good tracers of the stellar mass of a galaxy (Gilfanov 2004). Swartz, Soria, & Tennant (2008) found that ULXs tend to be relatively abundant in dwarf galaxies, suggesting that the ULX frequency per stellar mass decreases with increasing galaxian mass. In a sample of very nearby galaxies, Swartz, Tennant, & Soria (2009) found that the local environment ($100 \text{ pc} \times 100 \text{ pc}$) around the ULX tended to have bluer optical colors on average, indicating a link with young stellar populations. Based on these colors, they suggest that the most luminous ULXs are associated with early B-type stars with ages of $\approx 10 - 20$ Myrs. They argue that most ULXs are stellar mass black holes rather than more massive objects.

A recent survey of nearby galaxies suggests that there is a cut-off in the ULX X-ray luminosity function at high luminosities, with few sources above $2 \times 10^{40} \text{ erg/s}$ (Swartz et al. 2011). However, two recent studies have identified some extremely luminous ($\geq 10^{41} \text{ erg/s}$) X-ray point sources in more distant galaxies (Farrell et al. 2009; Sutton, Roberts, & Walton 2011). Such extreme luminosities can best be explained by intermediate mass black holes, as black holes with $\leq 80 M_{\odot}$ are not expected to produce such high luminosities (Swartz et al. 2011). Extending the current surveys of nearby galaxies to more distant and more luminous galaxies is critical to better constrain the upper end of this luminosity function.

There is some evidence that gravitational interactions between galaxies may increase the numbers of ULXs present in a galaxy. Studies of individual interacting and merging galaxies show that some have numerous ULXs (e.g., Arp 244, Zezas et al. 2002; Arp 284, Smith et al. 2005; NGC 3256, Lira et al. 2002; Arp 269, Roberts et al. 2002; Arp 270, Brassington et al. 2005; NGC 4410, Smith et al. 2003; the Cartwheel, Gao et al. 2003; Wolter, Trinchieri, & Colpi 2006; Crivellari, Wolter, & Trinchieri 2009). Since interacting galaxies tend to have enhanced star formation on average compared to normal galaxies (e.g., Bushouse 1987; Bushouse, Lamb, & Werner 1988; Kennicutt et al. 1987; Barton et al. 2000; Barton Gillespie, Geller, & Kenyon 2003; Smith et al. 2007; Ellison et al. 2008), one might expect enhanced ULX production in interacting systems if ULXs are associated with star formation.

Other conditions within interacting and merging galaxies may also increase the number of ULXs. For example, Soria & Wong (2006) have suggested that cloud collisions during galaxy interactions may lead to rapid, large-scale collapse of molecular clouds, producing a few massive protostars which quickly coalesce into a single star with mass $> 100 M_{\odot}$. This process may lead to an excess of ULXs in interacting systems. If intermediate mass black holes form in dense stellar clusters (Portegies Zwart et al. 2004a), and such clusters are more likely formed in interacting and merging galaxies due to increased gas pressure and enhanced cloud collisions, then ULXs might be expected to be found more commonly in interacting systems if such black holes contribute significantly to the ULX population. We note that in Arp 244 four ULX candidates are seen in the ‘overlap’ region where the two disks intersect (Zezas et al. 2002), a region where strong shocks and/or compression may be present. Alternatively, black hole fueling rates may be higher in interacting galaxies due to the more disturbed orbits of the interstellar clouds. Thus there are a number of theoretical ideas for why ULXs might be more common in interacting and merging galaxies.

In some interacting systems, X-ray sources have been found that are apparently associated with tidal features (Smith et al. 2005; Brassington et al. 2005). If there is a statistically-significant correlation between ULXs and tidal features, it would

imply that the environment of tidal features is particularly conducive to the formation of ULXs. On average, tidal features tend to have somewhat bluer UV/optical colors than their parent galaxies (Smith et al. 2010), possibly due to higher mass-normalized star formation. Strong gas compression and shocking can occur along tidal features (e.g., Gerber & Lamb 1994; Struck & Smith 2003), possibly inducing star formation and ULX creation.

In the current study, we present results from an archival *Chandra* survey of a large sample of interacting galaxies, comparing with available optical, UV, and infrared data. We use this database to investigate whether ULXs are more likely to occur in interacting galaxies than in normal systems, relative to the stellar mass and star formation rate, and whether they are more likely to occur in tidal features compared to disks. We also determined local UV/optical colors within the galaxies in the vicinity of the ULX to investigate the local stellar population. In addition, we use this dataset to determine the frequency of X-ray bright nuclei in interacting galaxies.

In Section 2 of this paper, we describe the galaxy sample, the *Chandra* datasets, and the ancillary UV, optical, and infrared data. In Section 3, we describe the ULX sample. In Section 4, we compare the number of ULXs with optical luminosity as a proxy for stellar mass, and in Section 5, we compare with previous studies of mostly spiral galaxies. In Section 6, we define a subset of strongly interacting galaxies and investigate their ULX properties. In Section 7 we compare with the far-infrared luminosity. We compare UV/optical colors in the vicinity of the ULX candidates to global colors of galaxies in Section 8. Finally, we obtain statistics on the frequency of X-ray detected nuclei in this sample compared to spiral samples in Section 9.

2. Sample Selection and Additional Data

To obtain a large enough sample of interacting galaxies for a statistical analysis of their ULXs, we started with the 338 systems in the Arp (1966) Atlas of Peculiar Galaxies. This Atlas contains most of the strongly interacting galaxies in the local Universe that are close enough for a detailed spatially-resolved analysis. Searching the *Chan-*

dra archives, we found that 95 Arp Atlas systems have archival ACIS-S or ACIS-I *Chandra* observations pointed at a location within $10'$ of the SIMBAD¹/NASA Extragalactic Database (NED²) coordinates of the system. We eliminated systems with sensitivities poorer than 10^{40} erg/s in the 0.5 – 8 keV range at the distance of the host galaxy, assuming a 10-count limit. For observations with the ACIS-S array, we only used datasets in which the S3 chip covered at least part of the Arp system. For ACIS-I observations, at least one of the four I array chips must have covered at least part of the Arp system for the system to be included in our sample. This ensures uniform sensitivity by omitting galaxies that are far off-axis. The aimpoint for the ACIS-S array is located in the S3 chip, so it has the highest sensitivity, while the aimpoint for the ACIS-I array is close to the center of the array, so no one chip is strongly favored in sensitivity.

We searched the Sloan Digitized Sky Survey (SDSS; Abazajian et al. 2003) archives for optical images of these galaxies. In our final sample, we only included galaxies which had calibrated SDSS Data Release 7 (DR7) images available. In some cases, the Arp system is split between two or three SDSS images. In these cases, we treated each SDSS image separately.

There were 45 Arp systems that fit these criteria. These systems are listed in Table 1, along with their positions, distances, and angular sizes. The distances were obtained from NED, using, as a first preference, the mean of the redshift-independent determinations, and as a second choice, $H_0 = 73$ km/s/Mpc, with Virgo, Great Attractor, and SA infall models. The angular size given is the total angular extent of the Arp system, obtained from NED, when available. Otherwise, it was estimated from the SDSS images or the Digital Sky Survey images available from NED. Most of these galaxies are relatively nearby, so *Chandra* provides good spatial information within the galaxies, yet most also have relatively small angular separations, so fit within the *Chandra* S3 $8'3 \times 8'3$ field of view.

There are a total of 69 individual galaxies in the 45 Arp systems, that are covered at least in part by the *Chandra* S3 or I array field of view. The names

¹<http://simbad.u-strasbg.fr>

²<http://nedwww.ipac.caltech.edu>

of the individual galaxies observed by Chandra are provided in Table 1. Of these 69 galaxies, 49 (69%) are classified as spirals in NED, 9 (13%) are irregular, and 8 (12%) are elliptical, with the rest peculiar or not typed. For most of the merger remnants in our sample (Arp 155, 160, 193, 215, 217, and 243), only a single nucleus is visible in near-infrared images (Rothberg & Joseph 2004; Haan et al. 2011) and in high spatial resolution radio continuum maps (Lucero & Young 2007; Parma et al. 1986; Krips 2007; Duric et al. 1986; Parra et al. 2010), thus we consider them a single galaxy for this study. For Arp 220, two nuclei are visible in near-infrared images (Graham et al. 1990) and radio images (Norris 1988), thus we consider it a galaxy pair. Arp 299 has three peaks in K band (Bushouse & Stanford 1992) and in the mid-infrared (Gehrz, Sramek, & Weedman 1983), all with counterparts in the radio continuum (Condon et al. 1982; Gehrz, Sramek, & Weedman 1983). However, follow-up multi-wavelength observations suggest that the third source may be an extranuclear star forming region rather than the nucleus of a third galaxy (Dudley & Wynn-Williams 1993; Imanishi & Nakanishi 2006; Alonso-Herrero et al. 2009). Thus we consider Arp 299 two galaxies rather than three. This information is used in Section 9 of this paper, when we determine the fraction of galactic nuclei in this sample that are detected in the X-ray. For Arp 189, the Chandra S3 field of view covers the tidal tail but not the main body of the galaxy. Four of the 69 galaxies are listed as Seyfert 1 or 2 in NED, 20 are listed as LINERs or transition objects (i.e., Sy/LINER or LINER/HII), and 17 are listed as having HII-type nuclear spectra. The nuclear spectral types are given in Table 1.

Table 1 also lists the *Chandra* exposure time and the corresponding X-ray point source luminosity (0.5 – 8 keV) detection limit assuming a 10-count limit. This limit was calculated using the Portable Interacting Multi-Mission Simulator (PIMMS; Mukai 1993) assuming an absorbed power law with spectral index $\Gamma = 1.7$ and Galactic HI column densities from Schlegel, Finkbeiner, & Davis (1998). In some cases, more than one *Chandra* observation is available for a given system. We generally used the dataset best-centered on the system, or the longest exposure.

We also searched the Galaxy Evolution Ex-

plorer (GALEX) archives for UV images of these galaxies, selecting only GALEX images with exposure times greater than 1000 sec. Of our 45 systems, 28 have appropriate GALEX images available. These systems are listed in Table 1, along with their GALEX exposure time. The GALEX NUV and FUV FWHM values are $5''.6$ and $4''.0$, respectively, and the GALEX pixels are $1''.5$ across. The field of view of the GALEX images is about $1'.2$ across. For comparison, the SDSS images have full width half maximum (FWHM) spatial resolutions between $0''.8$ and $2''.2$, pixel sizes of $0''.4$, and a field of view of $13'.6 \times 9'.9$.

We also obtained Infrared Astronomical Satellite (IRAS) total 60 and 100 μm flux densities for these systems from Rice et al. (1988), Surace, Sanders, & Mazzarella (2004), Xu & Lu (2003), or the xscanpi program³, being careful to include the total flux from the galaxy or galaxies covered by the Chandra field of view. The far-infrared luminosity of the included galaxy or galaxies for each Arp system is also provided in Table 1. These values were calculated using $L_{FIR} = 3.87 \times 10^5 D^2 (2.58 F_{60} + F_{100})$, where F_{60} and F_{100} are the 60 and 100 μm flux densities in Jy, D is the distance in Mpc, and L_{FIR} is in L_{\odot} . For Stephan’s Quintet (Arp 319), we excluded the flux from NGC 7320, which is a foreground galaxy. These luminosities are utilized in Section 7.

3. ULX Catalog

3.1. X-Ray Point Source Identification

Because of the wide range in X-ray sensitivities across our sample, individual X-ray sources may have few detected counts even though their estimated luminosities may be high. For this reason, we used three methods of source detection. First, we followed the data reduction procedure of Smith et al. (2005) using CIAO version 4.2 and the latest calibration files, additionally removing pixel randomization in creating the Level 2 event lists. On these datasets, we then used both the CIAO utility *wavdetect* and the source finding algorithm described in Tennant (2006) to find X-ray point sources. In addition, we used the Chandra Source Catalog (CSC; Evans et al. 2010) to search for X-ray point sources in these galaxies.

³<http://scanpiops.ipac.caltech.edu:9000/applications/Scanpi/>

In a few cases, sources listed in the CSC were not found as point sources by the source extraction routines listed above. These sources were generally listed as extended in the CSC, and appeared diffuse in the Level 2 event images, thus are not classified as ULXs. In addition, some sources were not included in the CSC because they lay on CCD chips that contained high levels of extended diffuse X-ray emission⁴. Others were not included in the CSC because the observations only became publicly available recently or were made in the spatially-restricted sub-array mode.

For the following analysis, we used the CSC determination of the ACIS aperture-corrected broadband (0.5 - 7 keV) flux, when available, after converting these values to 0.5 - 8.0 keV assuming a power law with photon index $\Gamma = 1.7$. Otherwise, the same procedure as was used to estimate detection limits was applied to the net observed source counts obtained from the Tennant (2006) source-finding results. In this work, we use the traditional definition of a ULX, with a 0.5 - 8 keV X-ray luminosity $\geq 10^{39}$ erg/s (e.g., Swartz et al. 2004). We corrected these X-ray fluxes for Galactic extinction using the Schlegel, Finkbeiner, & Davis (1998) Galactic HI column densities. Together, these two corrections are typically small, a $\sim 10\%$ effect. We did not correct for internal extinction. In most cases, the available archival X-ray data was not sensitive enough for a detailed spectroscopic analysis and derivation of the internal extinction. As noted by Swartz et al. (2004) and Swartz et al. (2011), correction for such internal extinction may increase the derived L_X values significantly for some objects.

3.2. Classification of the Candidate ULXs

As a first step in our analysis, we classified our X-ray sources as ‘tidal’, ‘disk’, ‘nuclear’ or ‘off-galaxy’ depending on their location relative to optical features. We used a cut-off of 2.5 counts above sky on the smoothed, sky-subtracted SDSS g images as our dividing line between ‘off-galaxy’ and ‘galaxy’. This corresponds to approximately 25.7 magnitudes/sq. arcsec, but this varies slightly from image to image.

For the systems observed with the ACIS-S array, we only included sources that lie within the

Chandra ACIS-S S3 chip field of view. In some datasets, other chips were read out as well, however, for consistency and for ease in determining the observed sky coverage needed to calculate background contamination, we only used sources in the S3 field of view. For the ACIS-I observations, we used sources in all four I-array chips.

The distinction between ‘disk’ and ‘tidal’ sources is sometimes ambiguous, as our determination of where the tail/bridge begins is subjective. This is especially true in the case of spiral arms, which may be tidally-disturbed by the interaction. In ambiguous cases, when the outer contours of the smoothed g band image showed a smoothly elliptical shape, we classified it as a spiral arm within a disk. In contrast, if considerable asymmetry was seen in the outermost contours, we classified the structure as tidal. As in Smith et al. (2007), we used multiple rectangular boxes to mark the extent of the tidal features and the disks. We used these boxes to decide whether a given source will be classified as tidal rather than disk.

X-ray point sources were identified as ‘nuclear’ if they were coincident within 6 SDSS pixels ($\leq 2''.4$) with the SDSS z-band peak in the inner disk of the galaxy. This is a conservative limit, as the 99% uncertainty in the Chandra absolute position for sources within $3'$ of the aimpoint is quoted as $0''.8^5$, while the astrometric accuracy of the SDSS images has been quoted as less than 1 pixel ($0''.4$) (Stoughton et al. 2002). In most cases, the X-ray/optical alignment of the nuclear sources is within $1''$, but for Arp 259 and 318, the offsets are $2''.4$. In these cases, it is possible that the sources may be truly non-nuclear, thus we may be inadvertently eliminating a few ULXs from the disk sample.

As an example to illustrate our classification scheme, in Figure 1 we display the smoothed SDSS g image of one of the Arp systems in our sample, Arp 259. The nuclear X-ray source is marked as a green circle, and the tidal ULX candidate is a yellow circle. The rectangular regions selected as disk are outlined in green, while the disk areas included are marked in red. The white contours mark 2.5 counts above the sky level, our dividing line between ‘sky’ and ‘galaxy’. According to Amram et al. (2007), this system consists of three

⁴see http://cxc.harvard.edu/csc/faq/dropped_chips.txt

⁵<http://asc.harvard.edu/cal/ASPECT/celmon/>

interacting galaxies. The tidal X-ray source is $\sim 3''$ from an optical knot.

3.3. X-Ray Source Sensitivity

As can be seen in Table 1, for 20 of the 45 Arp systems in the sample the sensitivity of the data is above the ULX luminosity cut-off of 10^{39} erg/s. Because there is a range in the sensitivities of the archival observations we are using, in the following analysis we divide the sample of galaxies into two subsets which we analyze separately. In the following discussion we refer to the original set of 45 Arp systems as the ‘intermediate sample’, while the subset of 25 systems with sensitivities $\leq 10^{39}$ erg/s we call the ‘sensitive sample’. We will use the sensitive sample to provide statistics on the total number of ULXs present, while the intermediate sample will be used to provide constraints on the top of the X-ray luminosity function ($\geq 10^{40}$ erg/s). From the X-ray luminosity functions presented in the literature for large samples of luminous extragalactic X-ray sources, a break or cut-off is indicated at about $1 - 2 \times 10^{40}$ erg/s (Grimm et al. 2003; Swartz et al. 2004, 2011; Liu 2011; Mineo et al. 2012). Thus 10^{39} erg/s is the ‘complete’ sample accounting for all the ULXs in the sample galaxies, while $\geq 10^{40}$ erg/s is the extreme luminous end of the ‘normal’ ULX population up to and above the luminosity function cut-off and may include extremely luminous examples similar to the hyperluminous object reported by Farrell et al. (2009).

In Table 2, we list the positions and 0.5 – 8 keV X-ray luminosities of the disk and tidal ULX candidates and the nuclear X-ray sources identified in this study. The off-galaxy X-ray sources are not included. These sources are assigned to the sensitive sample and/or the intermediate sample, depending upon which galaxy the sources are in, and the sensitivity of the Chandra observation of that galaxy. These assignments are provided in Table 2. Note that a source can belong to more than one sample, depending upon its luminosity and the sensitivity of the Chandra dataset. In Table 2 and in the subsequent analysis, we do not include X-ray sources with 10^{39} erg/s $\leq L_X < 10^{40}$ erg/s for galaxies that are not in the ‘sensitive sample’ (i.e., we do not include sources in this luminosity range for galaxies with sensitivities $> 10^{39}$ erg/s).

In Table 3, we list the numbers of Arp systems

in both the sensitive and intermediate samples, as well as the total number of individual galaxies in those systems that are included in the Chandra S3 or I array field of view. Table 3 also gives the mean distance to the Arp systems in the sample and the limiting L_X used for the sample. Various additional properties of the two sets of galaxies are also included in Table 3, and are discussed below.

In Table 3, we list the total number of disk, tidal, nuclear, and off-galaxy Chandra sources in each sample of galaxies, which have X-ray luminosities above the cut-off luminosity for that sample. In total, adding up over the two samples, and accounting for the fact that some ULXs can be in both the sensitive and intermediate samples, we have a total of 58 disk ULX candidates, 13 tidal sources, 26 nuclear sources, and 64 off-galaxy objects. No non-nuclear source in our sample of peculiar galaxies has $L_X > 10^{41}$ erg/s, thus we do not find any ULX candidates with the extreme luminosities of those found by Farrell et al. (2009) and Sutton, Roberts, & Walton (2011).

3.4. Optical Counterparts to X-ray Sources

We inspected the SDSS g images for optical counterparts to these X-ray sources. The disk and tidal ULX candidates with optical counterparts may be background objects such as quasars, active nuclei, or small angular size galaxies, or foreground stars. Alternatively, they may be ULXs associated with or located near compact knots of star formation or star clusters within the Arp galaxy. Sources with discrete optical counterparts are identified in Table 2, while the number of X-ray sources in each category that have optical counterparts is provided in Table 3. As shown in Table 3, the fraction of X-ray sources in the tails and disks that have optical counterparts are 0% to 44%, depending upon the sample, while 35% – 52% of the off-galaxy X-ray sources have optical counterparts.

For the off-galaxy sources with optical counterparts, we estimated optical magnitudes from the SDSS images and calculated the ratio of the X-ray flux to that in the optical, f_X/f_V , as defined by Maccacaro et al. (1988), converting to the 0.3 – 3.5 keV flux using PIMMS with photon index 1.7 and using the optical magnitude conversions of Jester et al. (2005). Almost all have $f_X/f_V \geq 0.3$, consistent with them being background AGN, though a few appear to be foreground stars, which

are expected to have lower f_X/f_V ratios (e.g., Maccacaro et al. 1988; Della Ceca et al. 2004).

For the disk/tidal ULX candidates, followup optical observations are needed to confirm whether apparent optical counterparts are indeed likely to be associated with the ULXs and to accurately determine galaxy-subtracted optical magnitudes.

3.5. Background Contamination

To properly compare the disk vs. tail/bridge numbers, we also need to correct for contamination by background sources. For background subtraction, we need an estimate of the surface area subtended by the tails/bridges vs. the disks. To this end, we counted the number of SDSS pixels within our tail/bridge vs. disk rectangular boxes, which are above our surface brightness cut-off level on the smoothed sky-subtracted g images (2.5 counts), that were also covered by either the Chandra S3 field of view (for ACIS-S observations) or any of the I chips (for ACIS-I observations). To accomplish this, we constructed a first mask of the sky, delineating the location of our rectangular disk/tidal boxes, a second mask, marking the location of the galaxy above the surface brightness cut-off, and a third mask, showing the field of view of the Chandra chip(s) in question. These three masks were then combined to create a single mask from which the number of relevant pixels was determined. These values were then converted into square arcminutes using the SDSS pixel size. In Table 3, for both samples of galaxies, we give the total surface area covered by the survey, in arcminutes. As expected, the area covered by the sensitive survey is less than that covered by the intermediate survey.

To estimate the amount of contamination of our ULX sample due to background X-ray sources, for each galaxy in each sample we calculated the flux corresponding to the selected L_X cut-off for that sample. We then estimated the number of probable background sources masquerading as ULXs for each galaxy by multiplying the observed area for each galaxy by the Moretti et al. (2003) determination of the number of background X-ray sources per area as a function of flux. We then summed over all of the galaxies in the respective sample to calculate the total expected number of background contaminants for that survey. These numbers are given in Table 3, along with the es-

timated fraction of the observed sources which are likely background objects. These percentages range from $\sim 20\%$ for the disk and tidal sources in the sensitive sample, to $31\% - 40\%$ for the intermediate sample. In Table 3, we also provide the background-corrected ULX counts in the disks and tails, after subtracting the expected number of interlopers.

4. Number of ULXs per SDSS Luminosity

Next, we scaled the background-corrected numbers of ULX sources by optical luminosity as a proxy for stellar mass, to determine whether ULXs are preferentially found in tidal regions or in inner disks. For this estimate, we used the SDSS r band flux. For a more direct comparison with the Swartz et al. (2004) study, which used B luminosities, we also calculated the SDSS g flux. We first sky-subtracted the SDSS images using the mean value from several rectangular sky regions far from the galaxies. We then determined the total SDSS r and g band fluxes within our defined ‘disk’ and ‘tidal’ rectangular boxes, including only pixels covered by the Chandra ACIS-S S3 field of view. We corrected these values for Galactic extinction as in Schlegel, Finkbeiner, & Davis (1998).

We then summed over all the tidal features in both samples of galaxies, to calculate the total r band luminosity of the portions of these features covered by the Chandra field of view. We repeated this process for the disks in each sample, and for the g band fluxes for the tails/bridges and the disks. The resultant disk and tail r and g band luminosities νL_ν for each sample are listed in Table 3. As can be seen in Table 3, $\sim 13\%$ of the total g and r light from the intermediate sample arises from tidal features. This is similar to the percentage found for the Smith et al. (2010) interacting sample.

Next, for both samples we compared the background-corrected number of ULX sources above the L_X limit for that sample with the r and g luminosities for that sample. In Table 3, we provide the ratio $N(\text{ULX})/L(\text{optical})$ for each sample, for the disks and tails separately. The uncertainties quoted throughout this paper are statistical uncertainties on the number of sources, calculated using the approximations for small numbers of events given by Gehrels (1986). These uncertain-

ties do not account for errors in the classification of sources or in the optical or X-ray luminosities.

These optical luminosities should be corrected for internal as well as Galactic extinction. Using $H\alpha/H\beta$ ratios, for two samples of nearby spiral galaxies Moustakas & Kennicutt (2006) and Moustakas et al. (2010) find median $E(B - V)$ values of 0.25 and 0.55, respectively, corresponding to A_r values of 0.7 and 1.5. For his sample of strongly interacting galaxies, Bushouse (1987) quotes a typical $E(B - V) \sim 0.3$, similar to the above values. For tidal tails and bridges, only a handful of $H\alpha/H\beta$ measurements of star forming regions are available (Duc et al. 1994, 2000; Mirabel et al. 1992; Werk et al. 2011), giving a median $A_r \sim 0.7$, but with considerable scatter. For the following calculations, we assume that, on average, galaxian disks suffer $\sim 35\%$ more extinction in the r band than tidal features, however, this is very approximate.

Using these estimates of extinction, in Table 3, we provide extinction-corrected values of $N(\text{ULX})/\nu L_\nu$. As above, the uncertainties here are only statistical uncertainties on the number of sources, and do not account for uncertainties in the extinction corrections, which can be substantial. In Table 3, for both samples, we provide the tidal-to-disk ratio of the extinction-corrected $N(\text{ULX})/\nu L_\nu(r)$ values. These show a slight enhancement in the tidal features compared to the disks. However, the uncertainties on the $N(\text{ULX})/\nu L_\nu$ values are very large. This is shown in Table 3 where we provide the difference between the tail and disk values, in terms of σ . These tail and disk values agree within 2.0σ . Furthermore, as noted earlier, there is some uncertainty in the classification of the ULX candidates as disk vs. tidal vs. off-galaxy vs. nuclear. Of our 11 tidal ULXs, four are located in the very extended and diffuse tidal features of Arp 215, for which the boundary between ‘tail’ and ‘off-galaxy’ is ambiguous in some cases. Furthermore, five of the remaining tidal ULX candidates are in Arp 270, near the boundary between ‘disk’ and ‘tidal’, so their classification is also uncertain. In addition, if some of the source classified as ‘nuclear’ are actually ‘disk’ sources, this will slightly decrease the difference between the disk and tidal sources. Also, if central AGNs contribute significantly to the observed optical light, correcting for that ef-

fect will tend to increase the $N(\text{ULX})/L(r)$ ratios of the disks compared to the tidal features.

In summary, we find a possible slight excess of ULXs associated with tidal features compared to the inner regions of these interacting galaxies. Such an enhancement is not unexpected, if ULX production is related to star formation. However, the uncertainties on this result are large, and we cannot rule out the possibility that tidal features have similar numbers of ULXs relative to their stellar masses as their parent disks.

5. Comparison to Spiral Galaxies

From a sample of 81 nearby galaxies with archival Chandra data available, Swartz et al. (2004) concluded that, on average, spiral galaxies have larger $N(\text{ULX})/L_B$ ratios than elliptical galaxies, implying more ULXs per stellar mass. To compare our sample to their results, we first need to convert our νL_ν values for the SDSS g band to the luminosity in the Johnson B band L_B . Using our summation over all the systems gives us an average $g - r$ for the disks of 0.51. For this color, the Windhorst et al. (1991) magnitude conversion relation gives $B = g + 0.816$. Combining this with the Zombeck (1990) conversion from absolute B magnitude to L_B and a similar equation for the g band gives $L_B = 0.486\nu L_\nu(g)$. After converting our luminosities, in Table 3 we provide $N(\text{ULX})/L_B$ ratios for the disks for our two samples.

For comparison, Swartz et al. (2004) found $N(\text{ULX})/L_B = 7.7 \pm 2.8 \times 10^{-44}$ ULX/(erg/s) for their spiral sample (after correction for a factor of 3.89 error in their original calculation). In a more recent study, Swartz et al. (2011) determined the number of ULXs per stellar mass for another sample of more nearby galaxies that was both volume-limited and magnitude-limited. This second sample, which includes mainly spirals and irregular galaxies, gives a slightly lower ULX-to-optical-light ratio, $N(\text{ULX})/L_B = 4.8 \pm 0.5 \times 10^{-44}$ (erg/s) $^{-1}$.

For comparison to our intermediate sample, we note that the Swartz et al. (2004) spiral sample has 10 out of 97 ULXs with $L_X \geq 10^{40}$ erg/s, giving $7.9 \pm \frac{3.4}{2.5} \times 10^{-45}$ (erg/s) $^{-1}$ in this luminosity range. In the Swartz et al. (2011) volume- and magnitude-limit sample, 19 out of 107 ULX candi-

dates have $L_X \geq 10^{40}$ erg/s, giving a similar value of $N(\text{ULX})/L_B = 8.5 \pm \frac{2.4}{1.9} \times 10^{-45} \text{ (erg/s)}^{-1}$.

In Table 3, we compare our $N(\text{ULX})/L_B$ values with the above values from Swartz et al. (2004) and Swartz et al. (2011). There is a significant excess of ULXs (a factor of 2.1 times higher ratio, a 3.0σ effect) in the sensitive Arp sample compared to the second control sample, but less of an excess compared to the first control sample. We conclude that, on average, our sample of Arp Atlas galaxies produce ULXs at a rate 1 – 2 times than that of spiral galaxies, relative to the optical luminosity and therefore the stellar mass.

6. ULX Statistics for Strong Interactions

The Arp Atlas contains many strongly interacting galaxies, but it also contains some systems that, although peculiar, may not have been strongly perturbed by a companion in the recent past. Thus it is possible that our statistics are being diluted by the presence of galaxies in the sample that are not strongly interacting.

To investigate this issue, from our original set of 45 Arp systems, we select a subset of strongly interacting systems. For each Arp system in the sample, we determined optical luminosity ratio(s) for the target galaxy or galaxies compared to the nearest neighbor(s), as well as galaxy separations relative to the diameter of the larger galaxy. These values were derived from the magnitudes, sizes, and coordinates available in NED, as well as inspection of the images in the Arp Atlas, SDSS, and Digitized Sky Survey (DSS). We define a galaxy as strongly interacting if the luminosity ratio is ≥ 1.4 and the pair separation is ≤ 2 diameters apart. We also include merger remnants with strong tails in the strongly interacting category, but exclude possible merger remnants without strong tidal tails (i.e., galaxies with shell-like structures or with faint tail-like features shorter than one disk diameter). This criteria gives us 22 Arp systems in our strongly interacting sample. These galaxies are identified in Table 1 by an asterisk.

We then subdivided this set further into sensitive and intermediate subsets based on the Chandra sensitivity criteria used earlier. The numbers of Arp systems and individual galaxies in these subsets are given in Table 4. For each of these subsets, in Table 4 we give the number of ULXs

above the 10^{39} and 10^{40} erg/s cutoffs, respectively. For each subset, we estimated the number of background sources, determined the respective g and r luminosities, and calculated $N(\text{ULX})/L(\text{optical})$. These values are also given in Table 4.

As in Table 3, in Table 4 we also provide comparisons between the tidal features and the disks, as well as with the Swartz et al. (2004) and Swartz et al. (2011) values. The difference between the $N(\text{ULX})/L(\text{optical})$ ratios of the disks and the tails/bridges is less than 2σ , thus we do not find strong evidence of an enhancement of this ratio in tidal features compared to disks.

However, we do find a $>2\sigma$ enhancement of a factor of 2.6 – 4.4 in the $N(\text{ULX})/L(\text{opt})$ in the Arp disks of the strongly interacting sensitive sample compared to the two control samples. An enhancement of this amount would not be surprising if ULX production is related to star formation. Interacting galaxies, on average, typically have mass-normalized star formation rates about two times larger than more normal galaxies (e.g., Bushouse 1987; Bushouse, Lamb, & Werner 1988; Kennicutt et al. 1987; Barton et al. 2000; Barton Gillespie, Geller, & Kenyon 2003; Smith et al. 2007).

However, there are other possible explanations. For example, the optical extinction may be larger in interacting galaxies on average than in normal spirals (Bushouse 1987; Bushouse, Lamb, & Werner 1988; Smith & Struck 2010), perhaps due to interstellar matter being driven into the central regions by the interaction. Bushouse (1987) found that $L_{\text{FIR}}/L_{H\alpha}$ for his sample of strongly interacting galaxies was a factor of $\sim 2.4 \times$ higher than for his control sample of normal spirals. If this is due solely to the optical extinction being higher in the interacting vs. the spiral galaxies, this may account for the higher $N(\text{ULX})/L(\text{optical})$ values in our strongly interacting sample.

7. Number of ULXs per FIR Luminosity

Our next goal is to compare the number of ULXs with the current rate of star formation in these galaxies. A standard method of estimating the star formation rate in galaxies is using the far-infrared luminosity (e.g., Kennicutt 1998). The far-infrared luminosities for most nearby galaxies are available from the IRAS satellite, however, this

has relatively low spatial resolution so generally just a total galaxian flux is available. If a pair of galaxies is relatively close together, IRAS will provide a measurement of the combined flux, but not individual fluxes. In some cases, if the pair of galaxies is widely separated, individual fluxes for galaxies in pairs is available.

For some of the galaxies in this study, the Chandra field of view is smaller than the angular size of the galaxy, so only part of the system is covered by Chandra. In those cases, we cannot provide a direct determination of the number of ULXs compared to the far-infrared luminosity. Of the 45 Arp systems in our sample, for 30 the Chandra field covered the whole galaxy or galaxies in question. Arp 169 was not observed by IRAS. For the remaining 29 systems, we can obtain both the total far-infrared luminosity and the total number of ULX sources, so can make a direct comparison. This sample of 29 Arp systems we call our IRAS subsample. These galaxies are identified in Table 1 in the L_{FIR} column. Of these 29 systems, 16 are in our ‘strongly interacting’ subset.

We then subdivided this IRAS sample into sensitive and intermediate subsets, based on their Chandra sensitivities as before. The number of Arp systems in these subsets is given in Table 5, along with the number of individual galaxies covered by the Chandra fields of view, the mean distance to the galaxies in each sample, and the sky areas covered. The number of disk, tail, nuclear, and off-galaxy X-ray point sources in each sample above their respective X-ray luminosity cut-offs are also given in Table 5, along with estimated numbers of background contaminants for each subsample and the number of X-ray sources with optical counterparts.

For each subset, the total (disk plus tidal) background-corrected number of non-nuclear ULXs associated with those systems $N(ULX)_{total}$ (excluding off-galaxy sources) was calculated, above the X-ray luminosity cut-off for that sample. Table 5 also provides the total far-infrared luminosity L_{FIR} for each subset, summing over all of the galaxies in the set. The final values of $N(ULX)_{total}/L_{FIR}$ are given in Table 5.

For comparison, the Swartz et al. (2004) sample had 55 galaxies of type S0/a or later, containing a total of 97 candidate ULXs. The total $L(FIR)$ for these galaxies is 1.5×10^{45} erg/s, giv-

ing $N(ULX)/L_{FIR} = 6.5 \pm 0.7 \times 10^{-44}$ (erg/s) $^{-1}$. For the volume-limited sample of Swartz et al. (2011), a similar ratio of $N(ULX)/L_{FIR} = 5.3 \pm 0.5 \times 10^{-44}$ (erg/s) $^{-1}$ was found. These differ from our values for the sensitive sample by less than 50% (Table 5), thus on average our Arp galaxies are producing ULXs at a similar rate relative to their star formation rates as spiral galaxies. This suggests that the rate of ULX production mainly depends upon the number of young stars present. Environmental effects such as enhanced cloud collisions, gas compression, and shocks in galaxy interactions may increase the rate of star formation and therefore the number of ULXs, but do not provide a large excess of ULXs above what is expected based on the number of young stars.

In the intermediate sample at limits of $\geq 10^{40}$ erg/s, however, our Arp systems appear quite deficient in ULXs relative to the far-infrared luminosities, compared to the spiral samples. Of the 97 ULX candidates in the Swartz et al. (2004) sample, 10 have $L_X \geq 10^{40}$ erg/s. This gives $N(ULX)/L_{FIR} = 6.7 \pm 2.9 \times 10^{-45}$ (erg/s) $^{-1}$ above $L_X \geq 10^{40}$ erg/s. In the more recent Swartz et al. (2011) sample, $N(ULX)/L_{FIR} = 9.4 \pm 2.2 \times 10^{-45}$ (erg/s) $^{-1}$ above $L_X \geq 10^{40}$ erg/s. Comparison with our value in Table 5, this implies a *deficiency* in ULXs in our intermediate sample relative to the far-infrared luminosities of approximately a factor of 7 – 10 compared to the comparison samples (a $\sim 2.7 - 3.8\sigma$ result).

Our intermediate sample contains several merger remnants that are extremely far-infrared-luminous, luminous enough to be classified as ‘luminous infrared galaxies’ (LIRGs) or ‘ultra-luminous infrared galaxies’ (ULIRGs), including Arp 193, 220, 240, 243, and 299 (see Table 1). These galaxies contribute high far-infrared luminosities to the total energy budgets for the intermediate sample in Table 5, however, they do not have many ULXs above the sensitivity limit of that sample. In contrast, the sensitive sample in Table 5 does not contain many extremely far-infrared luminous galaxies. The Swartz et al. (2004) and the Swartz et al. (2011) samples also do not contain any LIRGs or ULIRGs.

Our results for the intermediate sample implies that there is not a direct proportionality between the number of very luminous ULXs and the far-infrared luminosity compared to Swartz et al.

(2004, 2011). Instead, there is an apparent deficiency in high luminosity ULXs for very infrared-luminous galaxies. There are a couple of possible explanations for this. First, for some of these LIRGs and ULIRGs, an active galactic nucleus may be contributing significantly to powering the far-infrared luminosity. If this is the case, the far-infrared may not be directly proportional to the star formation rate. Note that some of the most IR-luminous systems in Table 1 are listed as Seyferts or transition objects. In some cases, mid-infrared spectra from the Spitzer telescope can provide an indirect estimate of the fraction of the total far-infrared luminosity that is powered by an active nucleus, via analysis of the mid-infrared spectral features. For Arp 193, 220, 243, and 299, such an analysis has been conducted, and the fraction of the observed far-infrared luminosity due to an active nucleus has been estimated to be less than 50% (Veilleux et al. 2009; Petric et al. 2011; Modica et al. 2012; Alonso-Herrero et al. 2012). Thus AGN domination of interstellar dust heating may not completely account for the deficiency in ULXs in these galaxies.

Another possibility is that in these galaxies ULXs are highly obscured in the X-ray, thus they are not detected above the X-ray flux limits of this survey with our assumptions about spectral shape. Recall that we are not correcting our ULX X-ray luminosities for internal extinction, which may cause us to underestimate the luminosities in some cases. For some starbursts, for example, M82, ULXs have been found to be very obscured. Another possibility is that the starbursts that power the far-infrared luminosity may be too young to have produced ULXs yet, if ULXs are associated with late O and early B stars with main sequence lifetimes of 10 – 20 Myrs.

Thus we conclude that for galaxies with moderate far-infrared luminosities, as in our sensitive sample, the number of ULXs is directly related to the far-infrared luminosity. However, at high L_{FIR} , the observed number of ULXs per L_{FIR} drops off. This is consistent with earlier studies comparing the galaxy-wide total X-ray luminosity to FIR luminosity in even more luminous LIRGs and ULIRGs, which show a deficiency in the X-ray at the high FIR end (Lehmer et al. 2010; Iwasawa et al. 2011).

8. Local UV/Optical Colors Near ULXs

Next, we determined the local UV/optical colors in the vicinity of the ULXs. After sky subtraction, we smoothed the SDSS and FUV images to the spatial resolution of the NUV images ($5''.6$ arcsec). At the location of each ULX candidate, we then determined the surface brightness at each UV/optical wavelength, binning and scaling the SDSS images to match the GALEX pixel size. At the distances of these galaxies (see Table 1), the $5''.6$ arcsec resolution of these images corresponds to 0.11 to 6.7 kpc. Thus the size scale of the ‘local environment’ we are studying in these galaxies varies quite a bit from galaxy to galaxy. Our ‘local’ regions are physically much larger than the 100 pc scale used in the Swartz et al. (2009) study, thus any correlation of ULXs with star formation may be more washed out in our sample compared to that study due to larger contributions from the surrounding stellar populations.

We did this analysis separately for the four classes of X-ray objects: disk sources, tail/bridge sources, nuclear sources, and off-galaxy sources. We merged the lists of ULX candidates from the sensitive and intermediate samples, removing duplicates. Histograms of these colors are shown in Figures 2 – 7, in the top, second, third, and fourth panels, respectively. In panels 1, 2, and 4 of Figures 2 – 7, we have plotted in red dotted histograms the local colors for the disk, tail, and off-galaxy sources with SDSS g optical point source counterparts.

In Figures 2 – 7, these histograms are compared with histograms for the global colors of the sample of normal spiral galaxies studied by Smith & Struck (2010) (sixth panel in each Figure), as well as those for the main disks of the ‘Spirals, Bridges, and Tails’ (SB&T) interacting galaxy sample studied by Smith et al. (2010) (fifth panel in each Figure). As seen in Figures 2 – 7 and as previously noted (Larson & Tinsley 1978; Schombert, Wallin, & Struck-Marcell 1990; Sol Alonso et al. 2006; Smith & Struck 2010), the optical/UV colors of interacting galaxies tend to have a larger dispersion than more normal galaxies, likely due to increased star formation combined with higher extinction.

In general, the local UV/optical colors in the vicinity of the disk ULX candidates (top panels in

Figures 2 – 7) have a larger dispersion than the global colors for the spiral galaxies (bottom panels), and in some cases, there is an apparent shift in the peak of the colors compared to spirals. In some cases, there is also more dispersion in the local colors near the disk ULXs compared to the global colors of the SB&T interacting sample. Interpreting the distributions of UV/optical colors of the local vicinities of the ULX candidates is difficult, since they are due to a combination of variations in local star formation properties and/or extinction, combined with possible contamination by UV/optically-bright background sources.

The distribution of colors for the off-galaxy sources may help identify possible background contaminants in the ULX samples. However, as is evident from the fourth panels in Figures 2 – 7, the distributions of colors of the local regions around the off-galaxy sources are very uncertain, due to numerous upper and lower limits. Furthermore, a large fraction of the off-galaxy sources were undetected in both bands of a color, thus are not included in these plots.

For the off-galaxy sources that are detected in both bands, the observed colors tend to have a larger spread compared to the global colors of spirals. The off-galaxy sources tend to be bluer than the global colors of galaxies in $u - g$, but redder in $FUV - NUV$ and $i - z$. For $g - r$ and $i - z$, the off-galaxy sources tend to have a large range of colors, both bluer and redder than the global colors of galaxies. As can be seen from Figures 2 – 7, the sources with discrete g band counterparts (marked by the red dotted histograms) tend to have a larger spread in colors than the sources without discrete point source optical counterparts, thus they are more likely to be background objects.

Perhaps the best color to use to identify background contaminants is $u - g$, since that shows the biggest difference in colors between galaxies as a whole and quasars/AGN. Richards et al. (2002) state that using an SDSS color limit of $u - g < 0.6$ is a good way to find quasars and AGN with $z \leq 2.2$. Consistent with this expectation, in Figure 4, most of the detected off-galaxy sources have $u - g < 0.6$, while the global colors of galaxies tend to be redder than this limit. Thus the ULX candidates with optical counterparts that have blue $u - g$ may be more likely to be background. However, this is not a definitive cut-off, since individual star

forming regions can also have $u - g < 0.6$; for example, in Arp 305, several clumps of star formation have $0.0 \leq u - g \leq 0.2$ (Hancock et al. 2009). Thus UV/optical color information alone is insufficient to definitively identify background sources, and followup spectroscopy is necessary to confirm that an object is a background source.

Even accounting for contamination by background sources, in some cases the spread in colors for the local regions is larger than for the global colors. This is particularly true for $u - g$, where the colors of the local regions around the ULX candidates are skewed blueward relative to global colors of both normal spirals and interacting galaxies (Figure 4). In Figure 4, 20 out of 58 (34%) of the disk ULX candidates have local $u - g < 0.6$, while almost none of the global colors of either the spirals or the interacting galaxies are this blue. This fraction is slightly higher than the expected fraction of background contaminants of about 25% (Table 3). Thus at least some of these very blue sources may be true ULXs, lying within regions containing younger stars.

There is also a shift to the blue in the peak of the $r - i$ distribution for the disk ULX locations compared to both spirals and interacting galaxies (Figure 6). For the disk ULX locations, 48% have $r - i < 0.2$, compared to 14% of the global colors of the normal spirals, and 22% of the global colors of the interacting galaxies. These differences are unlikely to be due solely to background contaminants, even assuming that the estimated 25% interlopers are all very blue.

For the other colors ($NUV - g$, $g - r$, $FUV - NUV$, and $i - z$) there is less difference between the colors of the ULX locations and the global colors of the interacting galaxies. The few discrepant sources may be background contaminants.

For the tidal ULX candidates (2nd panels in Figures 2 – 7), the dispersion in colors is generally larger than for the disk sources. Furthermore, in most colors there is an apparent shift to the blue in the mean color of the tidal regions compared to the spiral and interacting samples. This larger spread may be due in part to contamination by background sources. In general, a background object is likely to have a bigger effect on the optical/UV colors of a tail or bridge than a higher surface brightness galaxian disk.

However, even accounting for a possible 25% contamination rate, the colors of the ULX locations in the tidal features appear relatively blue. Approximately 38% of the tidal sources lie in regions with $u - g < 0.6$, bluer than most of the global colors. In $g - r$, 15% of the ULX candidate locations are bluer than $g - r = 0.2$, while almost none of the global colors are that blue. This suggests that the tidal ULXs are more likely to be associated with younger stellar populations. Another factor that may cause these colors to be somewhat bluer is that tidal features tend to have somewhat lower metallicities than inner disks, which may shift their colors bluewards.

9. Statistics on Nuclear Sources

The question of whether active galactic nuclei (AGN) are more common in interacting galaxies has been a topic of great interest in the astronomical community. Most previous studies have used optical spectroscopy to identify active galactic nuclei. Early studies suggested that there might be an excess of Seyferts in strongly interacting galaxies (Dahari 1985; Keel et al. 1985), but other studies did not find significant differences in the numbers of Seyferts among strongly interacting galaxies compared to more isolated systems (Bushouse 1986; Sekiguchi & Wolstencroft 1992; Donzelli & Pastoriza 2000; Casasola, Bettoni, & Galletta 2004; Ellison et al. 2008). Our Chandra study gives us an alternative way to investigate this question, via X-ray observations that are high enough spatial resolution to separate out nuclear emission. Note that not all nuclear X-ray emission may be due to an active galactic nucleus; some of this X-ray radiation may be from hot gas, ULXs, and/or X-ray binaries that are associated with a nuclear starburst. In selecting our X-ray sources (Section 3.1), we only chose objects that were point-like in the Chandra data, eliminating sources that are extended. In some cases (for example, Arp 220) the nuclear X-ray emission is extended (e.g., Ptak et al. 2003), but may contain a compact point source inside of diffuse hot gas. Thus our statistics on the nuclear X-ray point sources may be considered a lower limit, since we may be missing some sources.

The numbers of galactic nuclei in each of our samples that are detected in the X-ray above the

luminosity limit for that sample are given in Tables 3, 4, and 5. These are divided by the total number of individual galaxies in that sample, to obtain the percent of nuclei that are detected above that limit. These percentages are also given in Tables 3, 4, and 5. For these calculations we excluded Arp 189, for which the nucleus was not included in the Chandra S3 field of view.

Of the four sample galaxies classified as Seyfert 1 or 2 in NED, only one was detected in the X-ray above our flux limits (25%). Of the 20 LINER, Sy/LINER, or LINER/HII objects, four were detected above our flux cut-offs (20%). Six of the 20 galactic nuclei (35%) optically classified as HII-type were detected in the X-ray. In addition, three galaxies without nuclear spectral types in NED were detected by Chandra above our flux limits (11%). Thus the X-ray detection rates for these different spectral classes are similar.

To determine whether these percentages are higher than for more normal galaxies, for comparison we use the Zhang et al. (2009) sample of 187 nearby galaxies. Their sample is a combination of two samples of nearby galaxies, both Chandra archive-selected. The first component is a volume-limited sample of galaxies within 14.5 Mpc, that is also optical and infrared magnitude-limited. The second component is optical magnitude-limited and angular diameter-limited, and volume-limited to 15 Mpc. Morphologically, their combined sample contains 8% ellipticals, 13% dwarfs/irregulars, and the rest spirals. These percentages are similar to our sample (Section 2). Their combined sample is 8% Seyfert and 11% LINERs, based on optical spectroscopy. The overall percentage of active galaxies in our Arp sample is somewhat larger, with 6% Seyfert 1 or 2 and 29% LINER or transition objects, however, given the uncertainty in the NED classifications these percentages are not too inconsistent. Among our galaxies classified as strongly interacting, only one is listed as Seyfert 1 or 2 in NED (5%) and 13 are LINER or transition objects (59%). These percentages are slightly larger than in our original Arp sample.

Out of the 187 galaxies in the Zhang et al. (2009) sample, the nuclei of 29 ($15.5 \pm 3.5\%$) were detected by Chandra with an X-ray point source luminosity greater than 10^{39} erg/s. Above 10^{40} erg/s, 15 ($8.0 \pm 2.7\%$) were detected. Comparison of these numbers with our values in Table 3 show

that the nuclei of our original Arp Atlas sample of galaxies are detected at higher rates (about a factor of 2.3 – 3.9 times higher) than in this control sample. These differences are 1.7σ to 3.2σ . For the strongly interacting galaxies (Table 4), the percentages of nuclei that are detected are higher than the Zhang et al. (2009) values by a factor of $\sim 4 - 5$, differences of $1.3\sigma - 3.2\sigma$. Thus X-ray activity appears enhanced in the nuclei of interacting galaxies.

The probability that a galaxy is an AGN depends upon its mass and therefore its optical luminosity. To roughly account for possible differences in the masses and luminosities of the galaxies in the two samples, we scale the number of nuclear X-ray sources with the total optical luminosity of the sample, as we did earlier for the disk and tidal sources. In Tables 3 and 4, for each subset of galaxies we provide $N(\text{nuclear X-ray sources})/L_B(\text{total})$, the number of nuclear X-ray sources above the X-ray luminosity limit for that subset, divided by the total (disk plus tail) g luminosity, converted into B luminosities. As noted earlier (Section 7), for 15 out of the 45 Arp systems in our sample the Chandra fields of view do not cover the full extent of the galaxies. The optical luminosities quoted in Table 3 and 4 are not the total luminosities, but instead just the luminosities of the regions covered by the Chandra field of view. To scale with the number of nuclear sources, in Tables 3 and 4 we roughly correct for this difference, to include the entire luminosities of the galaxies in $N(\text{nuclear X-ray sources})/L_B(\text{total})$.

To compare with the Zhang et al. (2009) sample, we need to calculate blue luminosities for the Zhang et al. (2009) galaxies. To this end, we extracted blue magnitudes for the Zhang et al. (2009) galaxies from NED, preferentially using values from the Third Reference Catalogue of Bright Galaxies (RC3; de Vaucouleurs et al. 1991; Corwin, Buta, & de Vaucouleurs 1994), which were available for 94% of the galaxies. We then calculated blue luminosities for these galaxies using the distances in Zhang et al. (2009), along with $M_{B\odot} = 5.48$ and $L_{B\odot} = 1.9 \times 10^{33}$ erg/s. This gives a total L_B for the entire Zhang et al. (2009) sample of 1.97×10^{45} erg/s. Dividing this number into the number of central X-ray sources above the two luminosity cut-offs gives $N(\text{nuclear})/L_{B\text{total}}$ values as given in Tables 3 and

4. The above values for the Zhang et al. (2009) sample are consistent within 2σ uncertainties with the ratios for our samples (Tables 3 and 4). Thus we do not find strong evidence for enhancement of nuclear X-ray activity in interacting galaxies vs. normal galaxies when scaling by the blue luminosity.

We also compare the X-ray detection rate for the galactic nuclei in our sample with that of more luminous galaxies. For their sample of 17 LIRGs, Lehmer et al. (2010) found that nine nuclei were detected with $L_X \geq 10^{40}$ erg/s. This percentage of $53 \pm \frac{24}{17}\%$ is consistent with that for our strongly interacting sample. Their sample contains more optically-identified Seyferts than our sample (29%), but fewer LINER and transition objects (12%), giving a similar overall percentage of optically-defined active galaxies. For a higher redshift ($0.25 < z < 1.05$) sample of massive galaxies ($M_{\text{stellar}} > 2.5 \times 10^{10} M_{\odot}$), Silverman et al. (2011) determined the fraction of nuclei detected by Chandra with $L_X \geq 2 \times 10^{42}$ erg/s, a higher luminosity cut-off than we used for our sample. They found an enhancement of a factor of ~ 2 in their sample of close pairs, compared to a well-matched control sample.

As noted earlier, nuclear X-ray emission in the range we have studied, with $L_X < 10^{42}$ erg/s, is not necessarily from an AGN; a nuclear starburst may have an X-ray-bright nucleus due to hot gas, supernovae, ULXs, and/or multiple high mass X-ray binaries associated with the young stellar population. For example, the starburst nucleus of NGC 7714 is unresolved with Chandra at a distance of 37 Mpc, and has a 0.3 – 8 keV luminosity of 4.4×10^{40} erg/s (Smith et al. 2005). Since interactions may enhance nuclear star formation (e.g., Bushouse 1987), the star formation contribution to the X-ray flux from the nucleus may be stronger in our sample than in the Zhang et al. (2009) sample. It is also important to keep in mind that our sample of galaxies is significantly more distant than the Zhang et al. (2009) sample, thus in some cases circumnuclear star formation may contribute to our quoted nuclear X-ray luminosities. Possible differences in the morphological types of the galaxies in our sample and those in the Zhang et al. (2009) sample may also contribute to differences in nuclear detection rates, as early-type galaxies are more likely to have X-ray bright nuclei

than late-type (Zhang et al. 2009). In addition, our Arp sample and/or the Zhang et al. (2009) sample may be biased towards AGN since they are archive-selected, depending upon the original selection criteria for the original proposals.

10. Summary

We have identified 71 candidate ULXs in a set of 45 peculiar galaxy systems selected from the Arp Atlas to have both Chandra X-ray and SDSS optical images. We find a slight enhancement in the number of ULX sources normalized to the blue luminosity (a factor of \sim two higher) compared to earlier studies of spiral galaxies. This may be due to slightly enhanced star formation in these galaxies on average, if ULXs are associated with a young stellar population, or alternatively, to larger average optical extinctions in these galaxies. In the tidal features, we find an excess of ULX candidates per optical luminosity compared to the disks, though ambiguities in classification of these sources makes this result uncertain.

We also compared the number of ULXs with the far-infrared luminosities, which are an approximate measure of the star formation rate. For the Arp systems with the most sensitive Chandra observations, $N(\text{ULX})/L_{FIR}$ is consistent with that of spirals. This suggests that the ULX production rate in these systems is proportional to the number of young stars. However, when we extend our sample to include more distant Arp systems with higher far-infrared luminosities but less sensitive Chandra observations, we find a deficiency of high luminosity ULXs compared to the total far-infrared luminosity. In some of these infrared-luminous galaxies, an active galactic nucleus may contribute significantly to dust heating, lowering the $N(\text{ULX})/L_{FIR}$ ratio. Alternatively, ULXs may be more obscured in the X-ray in these extreme systems, most of which are merger remnants or very close pairs.

In comparing the UV/optical colors of the local vicinities of the ULX candidates with those of interacting galaxies as a whole, we do not find strong differences, with the exception of the $u - g$ and $r - i$ colors. In these colors, there appears to be an excess of blue colors in the vicinity of the ULX candidates compared to the global colors, that appears too large to be accounted for

solely by background contamination. The most likely explanation is that ULXs tend to lie in regions with relatively young stellar populations.

We also determined the number of galaxies with $L_X(\text{nuclear})$ greater than our sample luminosity limits, and compared with a control sample of nearby galaxies from Zhang et al. (2009). We found that a higher percentage of the nuclei were detected in our sample, particularly in the strongly interacting galaxies where $\sim 4 - 5 \times$ as many galaxies were detected than in the Zhang et al. (2009) sample. However, when we scale the number of X-ray detections with the blue luminosities of the galaxies we do not see a strong enhancement in our sample compared to the control sample.

We thank the anonymous referee for helpful suggestions that greatly improved this paper. We thank Qiongge Li and Nic Willis for help with downloading data, and Mark Hancock and Mark Giroux for helpful discussions. This work was funded by NASA Chandra grant AR9-0010A. D.A.S. is supported in part by NASA Chandra grants GO9-0098X and GO0-11099A. This work has made use of the NASA Chandra archives as well as the Chandra Source Catalog (CSC), provided by the Chandra X-ray Center (CXC) as part of the Chandra data archive. This research has made use of the NASA/IPAC Extragalactic Database (NED) and the NASA/IPAC Infrared Science Archive, which are operated by the Jet Propulsion Laboratory, California Institute of Technology, under contract with the National Aeronautics and Space Administration.

REFERENCES

- Abazajian, K., et al. 2003, *AJ*, 126, 2081
- Abolmasov, P. K., et al. 2007, *ApJ*, 668, 124
- Alonso-Herrero, A., et al. 2009, *ApJ*, 697, 660
- Alonso-Herrero, A., Pereira-Santaella, M., Rieke, G. H., & Rigopoulou, D. 2012, *ApJ*, 744, 2
- Amram, P., Mendes de Oliveira, C., Plana, H., Balkowski, C., & Hernandez, O. 2007, *A&A*, 471, 753
- Arp, H. 1966, *Atlas of Peculiar Galaxies* (Pasadena: Caltech)

- Barton, E. J., Geller, M. J., & Kenyon, S. J. 2000, *ApJ*, 530, 660
- Barton Gillespie, E., Geller, M. J., & Kenyon, S. J. 2003, *ApJ*, 582, 668
- Begelman, M. 2002, *ApJ*, 568, 97
- Belczynski, K., et al. 2006, *ApJ*, AJ, 133, 676
- Brassington, N. J., et al. 2005, *MNRAS*, 360, 801
- Bushouse, H. A. 1986, *AJ*, 91, 255
- Bushouse, H. A. 1987, *ApJ*, 320, 49
- Bushouse, H. A. & Stanford, S. A. 1992, *ApJS*, 79, 213
- Bushouse, H. A., Lamb, S. A., & Werner, M. W. 1988, *ApJ*, 335, 74
- Casosola, V., Bettoni, D., & Galleta, G. 2004, *A&A*, 422, 94
- Cardelli, J. A., Clayton, G. C., & Mathis, J. S. 1989, *ApJ*, 345, 245
- Colbert, E., & Mushotzky, R. 1999, *ApJ*, 519, 89
- Condon, J. J., Condon, M. A., Gisler, G., & Puschell, J. J. 1982, *ApJ*, 252, 102
- Corwin, H. G., Jr., Buta, R. J., and de Vaucouleurs, G. 1994, *AJ*, 108, 2128.
- Crivellari, E., Wolter, A., & Trinchieri, G. 2009, *A&A*, 501, 445
- Dahari, O. 1985, *ApJS*, 57, 643
- de Vaucouleurs, G., de Vacouleurs, A, Corwin, H. G., Buta, R. J., Fouque, P., and Paturel, G., *The Third Reference Catalogue of Bright Galaxies (RC3)*, Springer-Verlag.
- Della Ceca, R., et al. 2004, *A&A*, 428, 383
- Donzelli, C. J. & Pastoriza, M. G. 2000, *AJ*, 120, 189
- Duc, P.-A., Brinks, E., Springel, V., Pichardo, B., Weilbacher, P., & Mirabel, I. F. 2000, *AJ*, 120, 1238
- Duc, P.-A. & Mirabel, I. F. 1994, *A&A*, 289, 83
- Dudley, C. C. & Wynn-Williams, C. G. 1993, *ApJ*, 407, L65
- Duric, N., Seaquist, E. R., Crane, P. C., & Davis, L. E. 1986, *ApJ*, 304, 82
- Ellison, S. L., Patton, D. R., Simard, L., & McConnachie, A. W. 2008, *AJ*, 135, 1877
- Evans, I. N., et al. 2010, *ApJS*, 189, 37
- Freitag, M., Gürkan, M. A., & Rasio, F. A. 2006, *MNRAS*, 368, 141
- Farrell, S. A., Webb, N. A., Barret, D., Godet, O., & Rodrigues, J. M. 2009, *Nature*, 460, 73
- Gao, Y., Wang, Q. D., Appleton, P. N., & Lucas, R. A. 2003, *ApJ*, 596, L171
- Garrido, O., et al. 2002, *A&A*, 387, 821
- Gehrels, N. 1986, *ApJ*, 303, 336
- Gehrz, R. D., Sramek, R. A., & Weedman, D. W. 1983, *ApJ*, 267, 551
- Gerber, R. A., & Lamb, S. A. 1994, *ApJ*, 431, 604
- Gilfanov, M. 2004, *MNRAS*, 349, 146
- Grisé, F., Pakull, M. W., Soria, R., Motch, C., Smith, I. A., Ryder, S. D., & Böttcher, M. 2008, *A&A*, 486, 151
- Graham, J. R., Carico, D. P., Matthews, K., Neugebauer, G., Soifer, B. T., & Wilson, T. D. 1990, *ApJ*, 354, 5
- Grimm, H.-J., Gilfanov, M., & Sunyaev, R. 2003, *MNRAS*, 339, 793
- Haan, S., et al. 2011, *AJ*, 141, 100
- Hancock, M., Smith, B. J., Struck, C., Giroux, M. L., & Hurlock, S. 2009, *AJ*, 137, 4643
- Imanishi, M. & Nakanishi, K. 2006, *PASJ*, 58, 813
- Iwasawa, K., Sanders, D. B., Teng, S. H., et al. 2011, *A&A*, 529, A106
- Jester, S., et al. 2005, 130, 873
- Keel, W. C., Kennicutt, R. C., Jr., Hummel, E., & van der Hulst, J. M. 1985, *AJ*, 90, 708

- Kennicutt, R. C., Jr., Keel, W. C., van der Hulst, J. M., Hummel, E., & Roettiger, K. A. 1987, *AJ*, 93, 1011
- Kennicutt, R. C., Jr. 1998, *ApJ*, 498, 541
- King, A. R., et al. 2001, *ApJ*, 552, L109
- King, A. R. 2009, *MNRAS*, 393, L41
- Krips, M. 2007, *A&A*, 207, 464, 553
- Kuntz, K. D., Gruendl, R. A., Chu, Y.-H., Chen, C.-H. R., Still, M., Mukai, K., & Mushotzky, R. F. 2005, *ApJ*, 620, L31
- Larson, R. B. & Tinsley, B. M. 1978, *ApJ*, 219, 46
- Lehmer, B. D., Alexander, D. M., Bauer, F. E., et al. 2010, *ApJ*, 724, 559
- Lira, P., Ward, M., Zezas, A., Alonso-Herrero, A., & Ueno, S. 2002, *MNRAS*, 330, 259
- Liu, J.-F., Bregman, J. N., & Irwin, J. 2006, *ApJ*, 171
- Liu, J.-F., Bregman, J. N., & Seitzer, P. 2002, *ApJ*, 580, L31
- Liu, J.-F., Bregman, J. N., & Seitzer, P. 2002, *ApJ*, 602, 249
- Liu, J. 2011, *ApJS*, 192, 10
- Lucero, D. M. & Young, L. M. 2007, *AJ*, 134, 2148
- Maccacaro, T., Gioia, I. M., Wolter, A., Zamorani, G., & Stocke, J. T. 1988, *ApJ*, 328, 680
- Mineo, S., Gilfanov, M., & Sunyaev, R. 2012, *MNRAS*, 419, 2095
- Mirabel, I. F., et al. 1992, *A&A*, 256, L19
- Modica, F., et al. 2012, *AJ*, 143, 16
- Moustakas, J. & Kennicutt, R. C., Jr. 2006, *ApJ*, 651, 155
- Moustakas, J., Kennicutt, R. C., Jr., Tremonti, C. A., Dale, D. A., Smith, J.-D. T., & Calzetti, D. 2010, *ApJS*, 190, 233
- Moretti, A., Campana, S., Lazzati, D., & Tagliaferri, G. 2003, *ApJ*, 588, 696
- Mukai, K. 1993, *Legacy*, 3, 21
- Norris, R. P. 1988, 230, 345
- Pakull, M. W., Grisé, F., & Motch, C. 2006, in *IAU Symp. 230, Populations of High Energy Sources in Galaxies*, ed. E. J. A. Meurs & G. Fabbiano (Dordrecht: Kluwer), 293
- Pakull, M. W. & Mirioni, L. 2003, *RMxAC*, 15, 197
- Parma, P., Ruiter, H. R., Fanti, C., & Fanti, R. 1986, *A&AS*, 64, 135
- Parra, R., Conway, J. E., Aalto, S., Appleton, P. N., Norris, R. P., Pihlström, Y. M., & Kewley, L. J. 2010, *ApJ*, 720, 555
- Persic, M., & Rephaeli, Y. 2007, *A&A*, 463, 481
- Petric, A. O., et al. 2011, *ApJ*, 730, 28
- Portegies Zwart, S., et al. 2004a, *Nature*, 428, 1724
- Portegies Zwart, S., et al. 2004b, *MNRAS*, 355, 413
- Ptak, A., Colbert, E., van der Marel, R. P., Roye, E., Heckman, T., & Towne, B. 2006, *ApJS*, 166, 154
- Ptak, A., Heckman, T., Levenson, N. A., Weaver, K., & Strickland, D. 2003, *ApJ*, 592, 782
- Ranalli, P., Comastri, A., & Setti, G. 2003, *A&A*, 399, 39
- Rappaport, S. A., Podsiadlowski, P., & Pfahl, E. 2005, *MNRAS*, 356, 401
- Read, A. M. 2003, *MNRAS*, 342, 714
- Rice, W., Lonsdale, C. J., Soifer, B. T., Neugebauer, G., Kopan, E. L., Lloyd, L. A., de Jong, T., & Habing, H. J. 1988, *ApJS*, 68, 91
- Richards, G. T., et al. 2002, *AJ*, 123, 2945
- Roberts, T. P., Warwick, R. S., Ward, M. J., & Murray, S. S. 2002, *MNRAS*, 337, 677
- Roberts, T. P., Levan, A. J., & Goad, M. R. 2008, *MNRAS*, 387, 73
- Rothberg, B. & Joseph, R. D. 2004, *AJ*, 128, 2098
- Schlegel, D. J., Finkbeiner, D. P., & Davis, M. 1998, *ApJ*, 500, 525

- Schombert, J. M., Wallin, J. F., & Struck-Marcell, C. 1990, *AJ*, 99, 497
- Sekiguchi, K. & Wolstencroft, R. D. 1992, *MNRAS*, 255, 581
- Silverman, J. D., et al. 2011, *ApJ*, 743, 2
- Smith, B. J., Nowak, M., Donahue, M., & Stocke, J. 2003, *AJ*, 126, 1763
- Smith, B. J., Struck, C., & Nowak, M. 2005, *AJ*, 129, 1350
- Smith, B. J., Struck, C., Hancock, M., Appleton, P. N., Charmandaris, V., & Reach, W. T. 2007, *AJ*, 133, 791
- Smith, B. J., Giroux, M. L., Struck, C., Hancock, M., & Hurlock, S. 2010, *AJ*, 139, 1212; Erratum 2010, *AJ*, 139, 1212.
- Smith, B. J. & Struck, C. 2010, *AJ*, 140, 1975
- Stoughton, C., et al. 2002, *AJ*, 123, 485
- Sol Alonso, M., Lambas, D. G., Tissera, P., & Coldwell, G. 2006, *MNRAS*, 367, 1029
- Soria, R., & Motch, C. 2004, *A&A*, 422, 914
- Soria, R., & Wong, D. S. 2006, *MNRAS*, 372, 1531
- Struck, C., & Smith, B. J. 2003, *ApJ*, 589, 157
- Surace, J. A., Sanders, D. B., & Mazzarella, J. M. 2004, 127, 3235
- Sutton, A. D., Roberts, T. P., & Walton, D. J. 2011, *Astronomische Nachrichten*, 332, 362
- Swartz, D. 2006, *ApJ*, 651, L21
- Swartz, D. A., et al. 2004, *ApJS*, 154, 519
- Swartz, D. A., Soria, R., Tennant, A. F., & Yukita, M. 2011, *ApJ*, 741, 49
- Swartz, D. A., Soria, R., & Tennant, A. F. 2008, *ApJ*, 684, 282
- Swartz, D. A., Tennant, A. F., & Soria, R. 2009, *ApJ*, 703, 159
- Tao, L., Feng, H., Gris e, F., & Kaaret, P. 2011, *ApJ*, 737, 81
- Tennant, A. F. 2006, *AJ*, 132, 1372
- Terashima, Y., Inoue, H., & Wilson, A. S. 2006, *ApJ*, 645, 264
- Veilleux, S., et al. 2009, *ApJS*, 182, 628
- Werk, J., Putman, M., Meurer, G., & Santiago-Figueroa, N. 2011, *ApJ*, 735, 71
- Windhorst, R. W., et al. 1991, *ApJ*, 380, 362
- Wolter, A., Trinchieri, G., & Colpi, M. 2006, *MNRAS*, 373, 1627
- Xu, C. K. & Lu, N. 2003, *ApJ*, 595, 665
- Zezas, A., et al. 2002, *ApJ*, 577, 710
- Zhang, W. M., Soria, R., Zhang, S., Swartz, D. A., & Liu, J. 2009, *ApJ*, 699, 281
- Zombeck, M. V. 1990, *Handbook of Space Astronomy and Astrophysics*, second edition, Cambridge University Press.

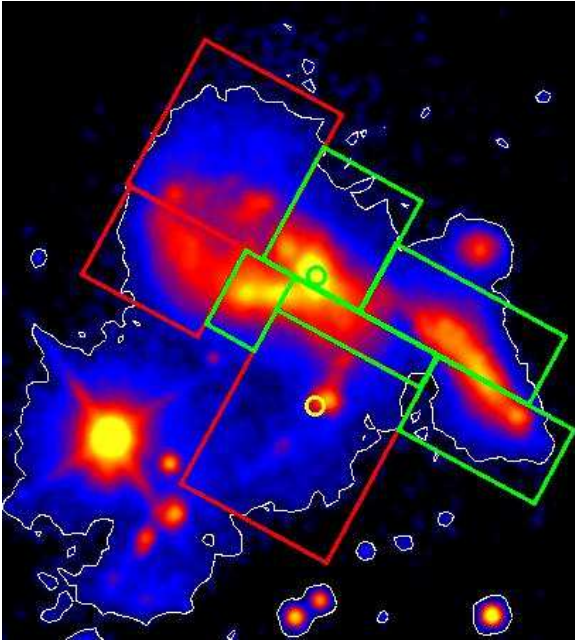


Fig. 1.— The smoothed g-band SDSS image of Arp 259, with ULX candidates marked. North is up and east to the left. The source marked in green is a disk ULX candidate, while the yellow circle marks the tidal source. The circles have $2''$ radii. The rectangular regions selected as disk are outlined in green, while the tail areas included are marked in red. The white contours mark 2.5 counts about the sky level, which we are using as our dividing point between ‘sky’ and ‘galaxy’. According to Amram et al. (2007), this system consists of three interacting galaxies.

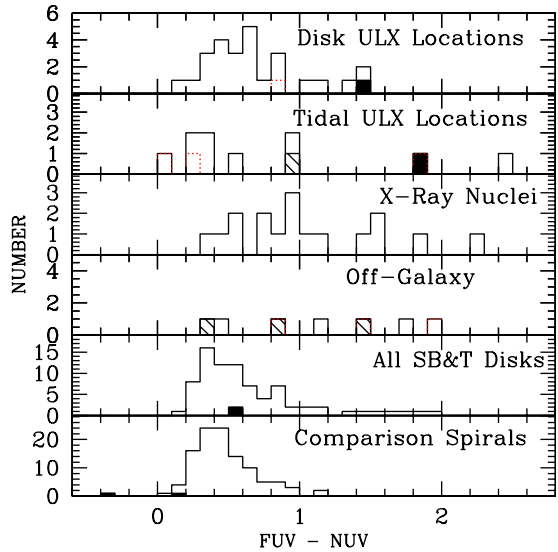


Fig. 2.— Histogram of the FUV – NUV colors for the ULX locations in the disks (top panel) and the tidal features (second panel), along with that for the X-ray bright galactic nuclei in the sample (third panel), and the off-galaxy locations (fourth panel). These are compared with global disk colors for the SB&T interacting galaxy sample in the fifth panel (from Smith et al. 2010) and normal spirals (from Smith & Struck 2010). The filled regions are lower limits and the hatched regions are upper limits. The red dotted histograms mark the sources with point source counterparts on the SDSS g image.

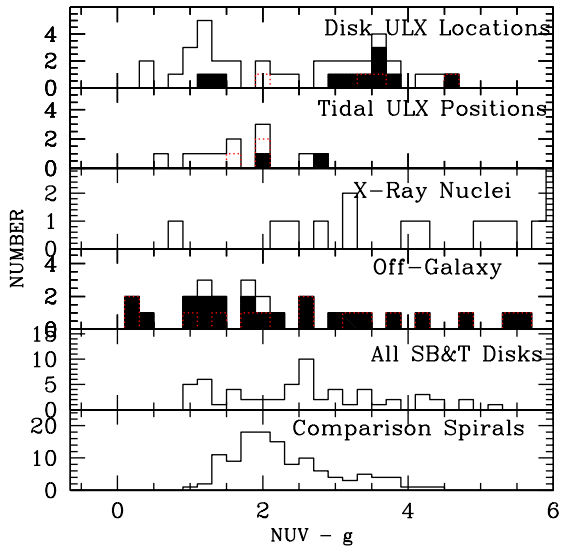


Fig. 3.— Histogram of $NUV - g$ colors as in Figure 2. The filled regions are lower limits. The red dotted histograms mark the sources with point source counterparts on the SDSS g image.

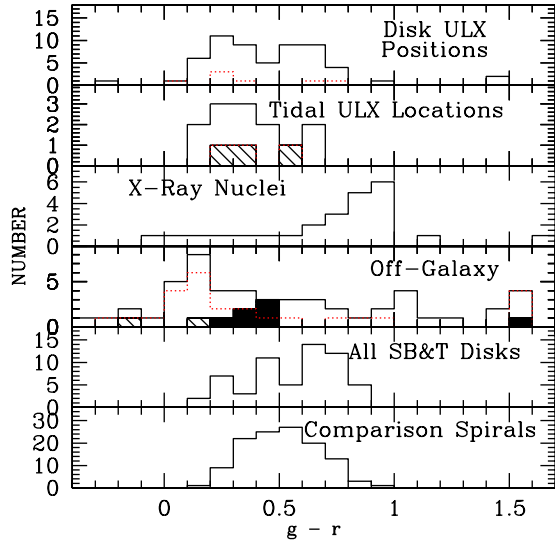


Fig. 5.— Histogram of $g - r$ colors as in Figure 2. The filled regions are lower limits and the hatched regions are upper limits. The red dotted histograms mark the sources with point source counterparts on the SDSS g image.

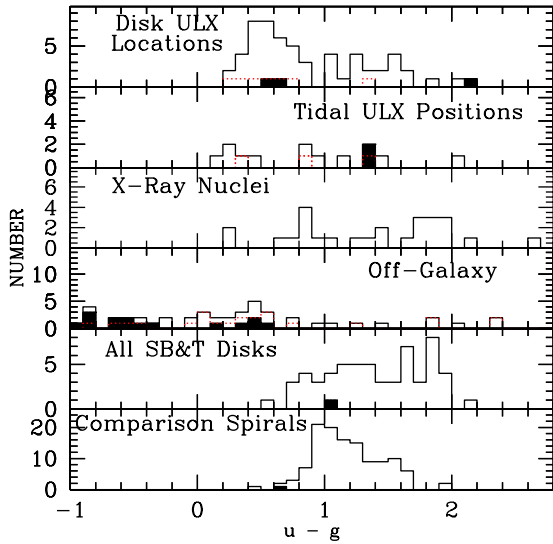


Fig. 4.— Histogram of $u - g$ colors as in Figure 2. The filled regions are lower limits. The red dotted histograms mark the sources with point source counterparts on the SDSS g image.

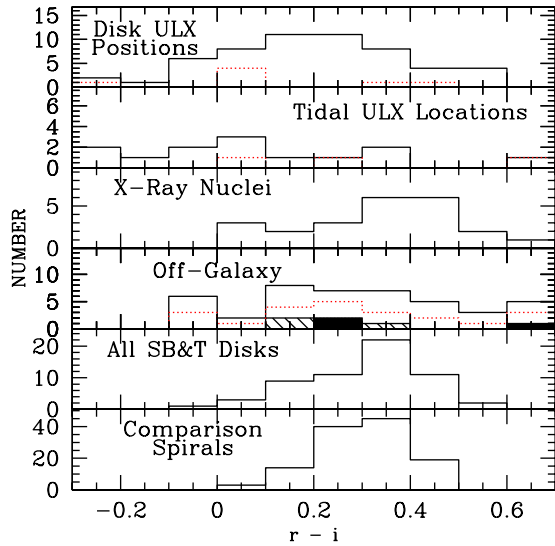


Fig. 6.— Histogram of $r - i$ colors as in Figure 2. The filled regions are lower limits and the hatched regions are upper limits. The red dotted histograms mark the sources with point source counterparts on the SDSS g image.

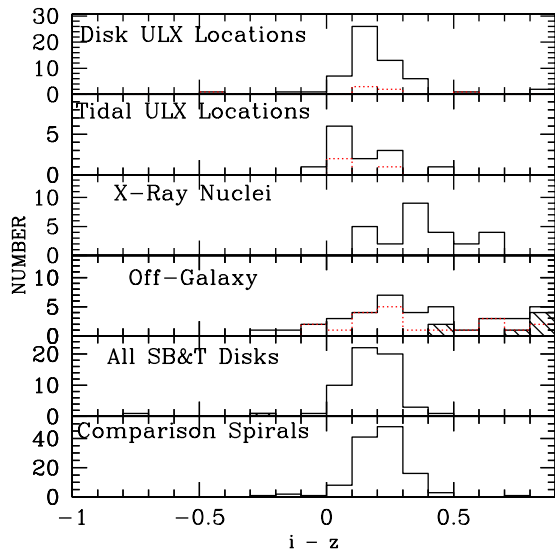


Fig. 7.— Histogram of $i - z$ colors as in Figure 2. The hatched regions are upper limits. The red dotted histograms mark the sources with point source counterparts on the SDSS g image.

TABLE 1
INTERACTING GALAXY SAMPLE FOR ULX STUDY AND AVAILABLE CHANDRA DATA

Arp Name	Observed Galaxy Name(s)	Nuclear Spectral Type	R.A. (J2000)	Dec. (J2000)	D [†] (Mpc)	Diameter [‡] (arcmin)	log ^{II} L _{FIR} (L _⊙)	Chandra Exposure Time (ksec)	L _X Limit (log [erg s ⁻¹])	Chandra Array	Chandra Dataset	GALEX FUV/NUV Exposure Times (sec)
Arp 16	M66	LINER/Sy2	11 20 15.0	+12 59 30	10	4 × 9	10.06	49.5	37.41	ACIS-S	09548	1680,3072
Arp 23	NGC 4618	HII	12 41 32.8	+41 9 3	7.3	3 × 4	8.72 ^a	54.8	37.09	ACIS-S	09549	3242,3242
Arp 24	NGC 3445/UGC 6021		10 54 40.1	+56 59 11	33	2 × 0.8	9.6 ^a	4.6	39.54	ACIS-I	01686	4118,4118
Arp 26	M101	HII	14 3 12.6	+54 20 57	7.2	27 × 29	9.46	56.2	37.07	ACIS-S	04731	1040,1040
Arp 27	NGC 3631		11 21 2.9	+53 10 10	22	5 × 5	9.99 ^a	89	37.84	ACIS-S	03951	1647,1647
Arp 37	M77	Sy2	2 42 40.7	-0 0 48	12	6 × 7	10.64	72.3	37.41	ACIS-S	00329	1616,1616
Arp 76	M90	LINER/Sy	12 36 49.8	+13 9 46	12	4 × 10	9.45	39.1	37.68	ACIS-S	05911	1598,4759
* Arp 84	NGC 5394/5	HII	13 58 35.8	+37 26 20	56	3.5 × 1.2	10.73	15.6	39.4	ACIS-S	10395	2820,4286
* Arp 91	NGC 5953/4		15 34 33.7	+15 11 49	34	1.7	10.33 ^a	9.9	39.18	ACIS-S	02930	
* Arp 94	NGC 3226	LINER	10 23 29.8	+19 52 54	20	6.0	9.48	2.2	39.36	ACIS-S	01616	
Arp 104	NGC 5216/8	Sy1,HII/LINER	13 32 8.9	+62 44 2	51	5.9 × 1.9	10.49 ^a	5.4	39.79	ACIS-S	10568	
Arp 116	NGC 4647/9	HII	12 43 36.0	+11 34 2	14	15	9.38	38.1	37.82	ACIS-S	00785	1658,1658
* Arp 120	NGC 4438	LINER	12 27 43.0	+13 2 38	14	10 × 8	9.23	25	38	ACIS-S	02883	6510,6510
Arp 134	M49	Sy2	12 29 46.7	+8 0 2	16	8 × 10	<7.98	39.5	37.92	ACIS-S	00321	
* Arp 147	IC 298		3 11 18.9	+1 18 53	129	0.4	10.21 ^a	24.5	39.96	ACIS-S	11280	
Arp 155	NGC 3656	LINER	11 23 38.8	+53 50 10	46	1.1 × 0.8	9.99 ^a	53.8	38.7	ACIS-S	10541	1647,1647
* Arp 160	NGC 4194	HII	12 14 9.5	+54 31 37	39	1 × 2	10.72 ^a	35.4	38.74	ACIS-S	07071	
Arp 162	NGC 3414	LINER	10 51 16.2	+27 58 30	25	3 × 4	8.62	13.7	38.77	ACIS-S	06779	
Arp 163	NGC 4670		12 45 17.2	+27 7 32	11	1 × 1	8.74 ^a	2.6	38.77	ACIS-S	07117	
* Arp 169		AGN	22 14 46.9	+13 50 24	108	2.3	-	27	39.84	ACIS-I	05635	7103,7104
Arp 189	NGC 4651	LINER	12 43 42.6	+16 23 36	27	3 × 4	9.94	24.7	38.58	ACIS-S	02096	2568,2568
* Arp 193	IC 883		13 20 35.3	+34 8 22	103	1.3 × 1.0	11.44 ^a	14	39.98	ACIS-S	07811	
Arp 206	UGC 5983/NGC 3432	LINER/HII	10 52 23.6	+36 36 24	13	6.6 × 1.0	9.38 ^a	1.9	39.05	ACIS-S	07091	
Arp 214	NGC 3718	Sy1/LINER	11 32 34.8	+53 4 5	17	4 × 8	8.74	4.9	38.87	ACIS-S	03993	1617,1617
* Arp 215	NGC 2782	Sy1/HII	9 14 5.1	+40 6 49	37	3 × 4	10.31 ^a	29.5	38.77	ACIS-S	03014	3459,3460
Arp 217	NGC 3310	HII	10 38 45.8	+53 30 12	18	2 × 3	10.23 ^a	47.1	37.94	ACIS-S	02939	
* Arp 220	Arp 220	LINER/HII/Sy2	15 34 57.1	+23 30 11	83	1 × 2	12.03 ^a	56.4	39.2	ACIS-S	00869	
Arp 233	UGC 5720	HII	10 32 31.9	+54 24 4	25	0.8 × 1	9.61 ^a	19.1	38.62	ACIS-S	09519	1680,1680
Arp 235	NGC 14		0 8 46.4	+15 48 56	13	2 × 3	8.75 ^a	4	38.74	ACIS-S	07127	
* Arp 240	NGC 5257/8	HII,HII/LINER	13 39 55.2	+0 50 13	102	3.0 × 1.1	11.29 ^a	19.9	39.82	ACIS-S	10565	
* Arp 242	NGC 4676A/B		12 47 10.1	+30 43 55	98	2 × 5	10.65 ^a	28.5	39.63	ACIS-S	02043	1700,1700
* Arp 243	NGC 2623	LINER/Sy2	8 38 24.1	+25 45 17	92	0.7 × 2	11.46 ^a	19.7	39.74	ACIS-S	04059	1696,4026
* Arp 247	IC 2338/9		8 23 33.5	+21 20 35	77	1.5	10.31 ^a	29.6	39.5	ACIS-I	07937	
* Arp 259	NGC 1741	HII,HII,HII	5 1 38.3	-4 15 25	55	1.4	10.33 ^a	35.5	39.04	ACIS-S	09405	1663,7558
* Arp 263	NGC 3239		10 25 4.9	+17 9 49	8.1	3 × 5	8.65 ^a	1.9	38.64	ACIS-S	07094	1766,1766
Arp 269	NGC 4485/90	HII,HII	12 30 33.6	+41 40 17	4.6	7 × 5	9.22 ^a	19.5	37.14	ACIS-S	01579	3247,4471
* Arp 270	NGC 3395/6	HII	10 49 52.6	+32 59 13	29	2 × 3	10.16 ^a	19.4	38.74	ACIS-S	02042	1487,2660
Arp 281	NGC 4627/4631	HII	12 42 3.8	+32 33 25	6.7	12 × 3	9.77	59.2	36.98	ACIS-S	00797	1680,1680
* Arp 283	NGC 2798/9	HII,HII	9 17 26.9	+41 59 48	30	3 × 3	10.48 ^a	5.1	39.35	ACIS-S	10567	2768,4272
* Arp 299	NGC 3690	HII/AGN,HII	11 28 30.4	+58 34 10	48	10 × 4	11.59 ^a	24.2	39.16	ACIS-I	01641	

TABLE 1—*Continued*

Arp Name	Observed Galaxy Name(s)	Nuclear Spectral Type	R.A. (J2000)			Dec. (J2000)			D [†] (Mpc)	Diameter [‡] (arcmin)	log ^{II} L _{FIR} (L _⊙)	Chandra Exposure Time (ksec)	L _X Limit (log [erg s ⁻¹])	Chandra Array	Chandra Dataset	GALEX FUV/NUV Exposure Times (sec)
* Arp 316	NGC 3190/3	LINER,LINER	10	18	0.5	+21	48	44	24	16.4	9.65	7.1	39.01	ACIS-S	11360	2078,2078
Arp 317	M65	LINER	11	19	41.3	+13	11	43	7.7	43 × 35	8.81 ^a	1.7	38.64	ACIS-S	01637	1650,1650
* Arp 318	NGC 835/8	Sy2/LINER,HII	2	9	31.3	-10	9	31	53	6.4	10.95	13.8	39.41	ACIS-S	10394	
* Arp 319	NGC 7317/8/9	Sy2	22	35	57.5	+33	57	36	89	3.2	10.15 ^a	19.7	39.73	ACIS-S	00789	1658,6761
Arp 337	M82	HII	9	55	52.7	+69	40	46	3.9	4 × 11	10.47 ^a	15.5	37.25	ACIS-I	01302	3075,3075

[†]From the NASA Extragalactic Database (NED), using, as a first preference, the mean of the distance-independent determinations, and as a second choice, $H_0 = 73$ km/s/Mpc, with Virgo, Great Attractor, and SA infall models. [‡]Total angular extent of Arp system. From NED, when available; otherwise, estimated from the SDSS images or the Digital Sky Survey images available from NED. ^{II}Total 42.4 – 122.5 μ m far-infrared luminosity. *In the strongly interacting subset (see Section 7). ^aIn the IRAS sample (see Section 8).

TABLE 2
TABLE OF ULX CANDIDATES AND NUCLEAR X-RAY SOURCES

Arp System	Location	CXO Name ¹ (J2000 Coordinates)	L_X (10^{39} erg/s) (0.5 – 8 keV)	Optical Source?	Sample(s) ²
Arp 16	disk	CXO J112018.3+125900	1.7		S
Arp 16	disk	CXO J112020.9+125846	11.6		I S
Arp 27	disk	CXO J112054.3+531040	24.5	yes	I S
Arp 27	disk	CXO J112103.0+531013	1.2		S
Arp 27	disk	CXO J112103.4+531048	2.1		S
Arp 27	disk	CXO J112109.5+530927	1.1		S
Arp 27	disk	CXO J112110.2+531012	2.1		S
Arp 27	disk	CXO J112112.7+531045	1.6	yes	S
Arp 37	nuclear	CXO J024240.8-000047	254.6		I S
Arp 76	disk	CXO J123653.6+131154	1.0		S
Arp 76	nuclear	CXO J123649.8+130946	4.0		S
Arp 84	nuclear	NEW J135837.9+372528	11.1		I
Arp 104	nuclear	NEW J133207.1+624202	25.0		I
Arp 116	disk	NEW J124337.3+113144	1.0	yes	S
Arp 120	nuclear	CXO J122745.6+130032	5.2		S
Arp 134	disk	CXO J122934.5+080032	1.2		S
Arp 134	disk	CXO J123006.6+080202	1.9		S
Arp 147	disk	NEW J031118.0+011902	10.0		I
Arp 147	nuclear	NEW J031119.5+011848	23.1		I
Arp 155	disk	NEW J112335.0+535002	1.6		S
Arp 155	disk	NEW J112336.2+535025	1.0		S
Arp 155	disk	NEW J112337.7+535042	1.2		S
Arp 155	disk	NEW J112341.7+535032	1.2		S
Arp 160	disk	CXO J121406.2+543143	12.8	yes	I S
Arp 160	disk	CXO J121408.7+543136	3.2		S
Arp 160	disk	CXO J121409.3+543127	1.6		S
Arp 160	disk	CXO J121409.3+543135	1.6		S
Arp 160	disk	CXO J121409.6+543139	1.1		S
Arp 160	nuclear	CXO J121409.6+543136	30.5		I S
Arp 160	tidal	CXO J121409.7+543215	12.0		I S
Arp 162	nuclear	NEW J105116.2+275830	23.1		I S
Arp 163	nuclear	CXO J124517.2+270731	1.3		S
Arp 169	nuclear	CXO J221445.0+135046	16.2		I
Arp 169	nuclear	CXO J221446.9+135027	55.9		I
Arp 193	nuclear	CXO J132035.3+340822	154.0		I
Arp 214	nuclear	NEW J113234.8+530404	53.5		I S
Arp 215	disk	CXO J091404.2+400738	2.5		S
Arp 215	disk	CXO J091404.4+400748	1.2		S
Arp 215	disk	CXO J091404.8+400650	5.2		S
Arp 215	disk	CXO J091405.1+400642	3.5		S
Arp 215	disk	CXO J091405.3+400628	2.9		S
Arp 215	disk	CXO J091405.4+400652	2.2		S
Arp 215	disk	CXO J091405.5+400648	1.4		S
Arp 215	disk	CXO J091410.9+400715	2.5		S
Arp 215	nuclear	CXO J091405.1+400648	41.7		I S
Arp 215	tidal	CXO J091408.3+400530	3.6	yes	S
Arp 215	tidal	CXO J091410.1+400619	1.0		S
Arp 215	tidal	CXO J091414.1+400701	1.2		S
Arp 215	tidal	CXO J091416.8+400659	2.2		S
Arp 217	disk	NEW J103843.3+533102	5.7		S
Arp 217	disk	NEW J103844.5+533005	1.4		S
Arp 217	disk	NEW J103844.6+533007	1.5		S
Arp 217	disk	NEW J103844.8+533004	3.7		S
Arp 217	disk	NEW J103846.0+533004	6.9		S
Arp 217	disk	NEW J103846.6+533038	1.8		S
Arp 217	disk	NEW J103846.7+533013	2.9		S

TABLE 2—*Continued*

Arp System	Location	CXO Name ¹ (J2000 Coordinates)	L _X (10 ³⁹ erg/s) (0.5 – 8 keV)	Optical Source?	Sample(s) ²
Arp 217	disk	NEW J103847.3+533028	5.1		S
Arp 217	disk	NEW J103850.2+532926	4.2		S
Arp 217	nuclear	NEW J103845.9+533012	8.5		S
Arp 233	disk	CXO J103232.0+542402	4.0	yes	S
Arp 240	disk	NEW J133953.5+005030	32.6	yes	I
Arp 240	disk	NEW J133958.8+005007	16.5		I
Arp 240	tidal	NEW J133955.9+004960	24.8		I
Arp 242	nuclear	CXO J124610.0+304355	23.4		I
Arp 242	nuclear	CXO J124611.2+304321	25.5		I
Arp 243	nuclear	CXO J083824.0+254516	92.6		I
Arp 247	disk	CXO J082333.7+212053	11.5		I
Arp 247	nuclear	CXO J082332.6+212017	13.4		I
Arp 259	nuclear	CXO J050137.7-041529	26.8		I
Arp 259	tidal	CXO J050137.7-041558	11.9		I
Arp 263	disk	CXO J102508.2+170948	1.3		S
Arp 269	disk	CXO J123030.4+414142	1.1		S
Arp 269	disk	CXO J123030.7+413911	1.0		S
Arp 269	disk	CXO J123032.1+413918	1.0		S
Arp 269	disk	CXO J123043.1+413818	1.1		S
Arp 270	disk	CXO J104949.4+325828	2.7		S
Arp 270	disk	CXO J104949.7+325838	5.3		S
Arp 270	disk	CXO J104949.8+325907	2.8		S
Arp 270	disk	CXO J104951.1+325833	2.4		S
Arp 270	nuclear	CXO J104955.0+325927	1.3		S
Arp 270	tidal	CXO J104946.6+325823	2.2		S
Arp 270	tidal	CXO J104947.4+330026	12.1		I S
Arp 270	tidal	CXO J104952.1+325903	4.7	yes	S
Arp 270	tidal	CXO J104953.2+325910	1.5		S
Arp 270	tidal	CXO J104959.3+325916	1.2		S
Arp 281	disk	CXO J124155.5+323216	2.1		S
Arp 281	disk	CXO J124211.1+323235	1.6		S
Arp 299	disk	NEW J112831.0+583341	16.1	yes	I
Arp 316	nuclear	CXO J101805.6+214956	10.4		I
Arp 317	disk	CXO J111858.4+130530	1.2		S
Arp 318	nuclear	CXO J020924.5-100808	45.2		I
Arp 318	nuclear	CXO J020938.5-100848	157.6		I
Arp 319	disk	NEW J223603.7+335825	14.2		I
Arp 319	nuclear	NEW J223556.7+335756	12.3		I
Arp 319	nuclear	NEW J223603.6+335833	296.9		I
Arp 319	tidal	NEW J223555.7+335739	23.1	yes	I
Arp 337	disk	NEW J095550.2+694047	1.4		S

¹Sources labeled ‘new’ are not in the current version of the Chandra Source Catalog. ²I: In the intermediate sample. S: In the sensitive sample.

TABLE 3
RESULTS ON ULX CANDIDATES

		Sensitive Sample	Intermediate Sample
General Properties	L_X (limit) (erg/s)	1×10^{39}	1×10^{40}
	Number Arp Systems	25	45
	Number Individual Galaxies	29	69
	Mean Distance (Mpc)	16.6	37.6
	Disk Area (arcmin ²)	791.8	901.2
	Tail Area (arcmin ²)	59.8	91.4
	Off-Galaxy Area (arcmin ²)	846.5	1911.0
Disk Sources	Number X-Ray Sources $\geq L_X$ (limit)	52	9
	Number $\geq L_X$ (limit) w/ Optical Counterparts	5	4
	Percent $\geq L_X$ (limit) w/ Optical Counterparts	9%	44%
	Estimated Number Background $\geq L_X$ (limit)	9.8	2.8
	Percent Background Contaminants $\geq L_X$ (limit)	18%	31%
	Background-Corrected Number $\geq L_X$ (limit)	42.2	6.2
Tidal Sources	Number X-Ray Sources $\geq L_X$ (limit)	10	5
	Number $\geq L_X$ (limit) w/ Optical Counterparts	2	1
	Percent $\geq L_X$ (limit) w/ Optical Counterparts	20%	20%
	Estimated Number Background $\geq L_X$ (limit)	2.3	2.0
	Percent Background Contamination $\geq L_X$ (limit)	23%	40%
	Background-Corrected Number $\geq L_X$ (limit)	7.7	3.0
Nuclear Sources	Number X-Ray Sources $\geq L_X$ (limit)	10	21
Off-Galaxy Sources	Number Sources $\geq L_X$ (limit)	38	28
	Number $\geq L_X$ (limit) w/ Optical Counterparts	20	10
	Percent $\geq L_X$ (limit) w/ Optical Counterparts	52%	35%
Optical Luminosities (10^{44} erg/s)	νL_ν (r)(disk)	11.65	34.78
	νL_ν (r)(tail)	0.59	5.12
	νL_ν (g)(disk)	8.76	25.75
	νL_ν (g)(tail)	0.52	4.17
Disks vs. Tails N(ULX)/L(opt) (10^{-46} (erg/s) ⁻¹)	Bkgd-corrected N(ULX)/ νL_ν (r)(disk)	361.8 ± 70.9	17.7 ± 11.9
	Bkgd-corrected N(ULX)/ νL_ν (r)(tail)	1300.7 ± 523.4	58.5 ± 66.3
	Bkgd-corrected N(ULX)/ νL_ν (g)(disk)	481.3 ± 94.3	23.9 ± 16.0
	Bkgd-corrected N(ULX)/ νL_ν (g)(tail)	1488.8 ± 828.1	72.0 ± 81.6
	Bkgd- and extinction-corrected N(ULX)/ νL_ν (r)(disk)	134.0 ± 26.3	6.6 ± 3.1
	Bkgd- and extinction-corrected N(ULX)/ νL_ν (r)(tail)	660.24 ± 367.2	29.71 ± 33.7
	Ratio Tail/Disk N(ULX)/ νL_ν (r)	4.9 ± 2.9	4.5 ± 5.4
	Sigma Difference Tail vs. Disk N(ULX)/ νL_ν (r)	2.0	1.1
Arp Disks vs. Other Samples Bkgd-corrected N(ULX)/L_B (disk) (10^{-46} (erg/s) ⁻¹)	Arp Disks	990.3 ± 194.0	49.2 ± 32.9
	Swartz et al. (2004)	770.0 ± 280.0	79.4 ± 34.0
	Ratio Arp Disks vs. Swartz et al. (2004)	1.3 ± 0.4	0.6 ± 0.5
	Sigma Difference Arp Disks vs. Swartz et al. (2004)	0.7	0.7
	Swartz et al. (2011)	480.0 ± 50.0	85.2 ± 24.4
	Ratio Arp Disks vs. Swartz et al. (2011)	2.1 ± 0.4	0.6 ± 0.3
Sigma Difference Arp Disks vs. Swartz et al. (2011)	2.9	0.9	
Nuclear Detections Arp Galaxies vs. Other Samples (10^{-46} (erg/s) ⁻¹)	Arp Galaxies Percent Nuclei Detected	35.7 ± 15.3	30.9 ± 8.3
	Zhang et al. (2009) Percent Nuclei Detected	15.5 ± 3.5	8.0 ± 2.7
	Ratio Percentage Arp Galaxies vs. Zhang et al. (2009)	2.3 ± 1.1	3.9 ± 1.4
	Sigma Difference Arp Galaxies vs. Zhang et al. (2009)	1.7	3.2
	Arp Galaxies N(nuclear X-ray sources)/L _B	192.8 ± 82.5	125.6 ± 33.9
	Zhang et al. (2009) N(nuclear X-ray sources)/L _B	147.2 ± 32.8	76.1 ± 25.2
	Ratio N(nuclear)/L _B Arp Galaxies vs. Zhang et al. (2009)	1.3 ± 0.6	1.6 ± 0.7
	Sigma Difference Arp Galaxies vs. Zhang et al. (2009)	0.7	1.3

TABLE 4
RESULTS ON ULX CANDIDATES: STRONGLY INTERACTING SUBSET OF GALAXIES

		Sensitive Sample	Intermediate Sample
General Properties	L_X (limit) (erg/s)	1×10^{39}	1×10^{40}
	Number Arp Systems	5	22
	Number Individual Galaxies	6	40
	Mean Distance (Mpc)	21.2	57.7
	Disk Area (arcmin ²)	56.4	132.9
	Tail Area (arcmin ²)	29.7	55.9
	Off-Galaxy Area (arcmin ²)	244.0	1101.2
Disk Sources	Number X-Ray Sources $\geq L_X$ (limit)	18	7
	Number $\geq L_X$ (limit) w/ Optical Counterparts	1	3
	Percent $\geq L_X$ (limit) w/ Optical Counterparts	5%	42%
	Estimated Number Background $\geq L_X$ (limit)	2.0	2.4
	Percent Background Contaminants $\geq L_X$ (limit)	11%	34%
	Background-Corrected Number $\geq L_X$ (limit)	16.0	4.6
Tidal Sources	Number X-Ray Sources $\geq L_X$ (limit)	10	5
	Number $\geq L_X$ (limit) w/ Optical Counterparts	2	1
	Percent $\geq L_X$ (limit) w/ Optical Counterparts	20%	20%
	Estimated Number Background $\geq L_X$ (limit)	1.4	1.9
	Percent Background Contamination $\geq L_X$ (limit)	13%	38%
	Background-Corrected Number $\geq L_X$ (limit)	8.6	3.1
Nuclear Sources	Number X-Ray Sources $\geq L_X$ (limit)	4	17
Off-Galaxy Sources	Number Sources $\geq L_X$ (limit)	23	27
	Number $\geq L_X$ (limit) w/ Optical Counterparts	10	9
	Percent $\geq L_X$ (limit) w/ Optical Counterparts	43%	33%
	Estimated Number Background $\geq L_X$ (limit)	24.8	57.0
	Percent Observed/Expected Off-Galaxy $\geq L_X$ (limit)	92%	47%
Optical Luminosities (10^{44} erg/s)	νL_ν (r)(disk)	1.94	23.46
	νL_ν (r)(tail)	0.44	4.85
	νL_ν (g)(disk)	1.66	17.48
	νL_ν (g)(tail)	0.38	3.93
Disks vs. Tails N(ULX)/L(opt) (10^{-46} (erg/s) ⁻¹)	Bkgd-corrected N(ULX)/ νL_ν (r)(disk)	822.5 ± 274.5	19.6 ± 16.1
	Bkgd-corrected N(ULX)/ νL_ν (r)(tail)	1962.7 ± 371.3	63.5 ± 11.0
	Bkgd-corrected N(ULX)/ νL_ν (g)(disk)	961.2 ± 320.7	26.2 ± 14.7
	Bkgd-corrected N(ULX)/ νL_ν (g)(tail)	2279.5 ± 1128.7	78.4 ± 36.5
	Bkgd- and extinction-corrected N(ULX)/ νL_ν (r)(disk)	304.6 ± 101.7	7.2 ± 6.0
	Bkgd- and extinction-corrected N(ULX)/ νL_ν (r)(tail)	996.30 ± 80.1	32.25 ± 4.1
	Ratio Tail/Disk N(ULX)/ νL_ν (r)	3.3 ± 1.8	4.5 ± 5.3
	Sigma Difference Tail vs. Disk N(ULX)/ νL_ν (r)	1.9	1.1
Arp Disks vs. Other Samples Bkgd-corrected N(ULX)/L_B (disk) (10^{-46} (erg/s) ⁻¹)	Arp Disks	1977.7 ± 659.9	54.0 ± 34.5
	Swartz et al. (2004)	770.0 ± 519.9	79.4 ± 30.3
	Ratio Arp Disks vs. Swartz et al. (2004)	2.6 ± 0.9	0.7 ± 24.6
	Sigma Difference Arp Disks vs. Swartz et al. (2004)	2.3	0.5
	Swartz et al. (2011)	480.0 ± 50.0	85.2 ± 19.4
	Ratio Arp Disks vs. Swartz et al. (2011)	4.1 ± 1.4	0.6 ± 0.5
Nuclear Detections Arp Galaxies vs. Other Samples (10^{-46} (erg/s) ⁻¹)	Sigma Difference Arp Disks vs. Swartz et al. (2011)	2.9	0.6
	Arp Galaxies Percent Nuclei Detected	66.7 ± 33.3	42.5 ± 13.4
	Zhang et al. (2009) Percent Nuclei Detected	15.5 ± 3.5	8.0 ± 10.5
	Ratio Percentage Arp Galaxies vs. Zhang et al. (2009)	4.3 ± 2.3	5.3 ± 2.7
	Sigma Difference Arp Galaxies vs. Zhang et al. (2009)	1.3	3.2
	Arp Galaxies N(nuclear X-ray sources)/L _B	350.7 ± 278.7	142.1 ± 43.6
Zhang et al. (2009) N(nuclear X-ray sources)/L _B	147.2 ± 167.8	76.1 ± 34.1	
Ratio N(nuclear)/L _B Arp Galaxies vs. Zhang et al. (2009)	2.4 ± 1.9	1.9 ± 0.7	
Sigma Difference Arp Galaxies vs. Zhang et al. (2009)	1.2	1.6	

TABLE 5
RESULTS ON ULX CANDIDATES: COMPARISON WITH IRAS

		Sensitive Sample	Intermediate Sample
General Properties	L_X (limit) (erg/s)	1×10^{39}	1×10^{40}
	Number Arp Systems	14	29
	Number Individual Galaxies	16	47
	Mean Distance (Mpc)	18.1	43.6
	Disk Area (arcmin ²)	158.4	218.2
	Tail Area (arcmin ²)	43.4	72.3
	Off-Galaxy Area (arcmin ²)	676.3	1560.2
Disk Sources	Number X-Ray Sources $\geq L_X$ (limit)	44	8
	Number $\geq L_X$ (limit) w/ Optical Counterparts	4	4
	Percent $\geq L_X$ (limit) w/ Optical Counterparts	9%	50%
	Estimated Number Background $\geq L_X$ (limit)	3.2	1.3
	Percent Background Contaminants $\geq L_X$ (limit)	7%	15%
	Background-Corrected Number $\geq L_X$ (limit)	40.8	6.7
Tidal Sources	Number X-Ray Sources $\geq L_X$ (limit)	10	5
	Number $\geq L_X$ (limit) w/ Optical Counterparts	2	1
	Percent $\geq L_X$ (limit) w/ Optical Counterparts	20%	20%
	Estimated Number Background $\geq L_X$ (limit)	1.9	1.9
	Percent Background Contamination $\geq L_X$ (limit)	19%	38%
	Background-Corrected Number $\geq L_X$ (limit)	8.1	3.1
Nuclear Sources	Number X-Ray Sources $\geq L_X$ (limit)	5	12
Off-Galaxy Sources	Number Sources $\geq L_X$ (limit)	36	21
	Number $\geq L_X$ (limit) w/ Optical Counterparts	19	7
	Percent $\geq L_X$ (limit) w/ Optical Counterparts	52%	33%
	Estimated Number Background $\geq L_X$ (limit)	43.9	44.8
	Percent Observed/Expected Off-Galaxy $\geq L_X$ (limit)	82%	46%
Disk+Tidal (10^{-47} (erg/s) ⁻¹)	Arp Galaxies L(FIR) (10^{44} erg/s)	6.39	102.33
	Arp Galaxies N(ULX)/L(FIR)	$7649.0 \pm^{1315.1}_{1146.6}$	$95.7 \pm^{46.0}_{34.7}$
	Swartz et al. (2004) N(ULX)/L(FIR)	$6466.7 \pm^{725.8}_{655.3}$	$666.7 \pm^{285.2}_{206.9}$
	ratio Arp vs. Swartz et al. (2004) N(ULX)/L(FIR)	$1.2 \pm^{0.2}_{0.2}$	$0.14 \pm^{0.08}_{0.08}$
	sigma Difference Arp vs. Swartz et al. (2004) N(ULX)/L(FIR)	0.9	2.7
	Swartz et al. (2011) N(ULX)/L(FIR)	5300.0 ± 500.0	940.0 ± 220.0
	ratio Arp vs. Swartz et al. (2011) N(ULX)/L(FIR)	$1.4 \pm^{0.2}_{0.2}$	$0.10 \pm^{0.05}_{0.05}$
	sigma Difference Arp vs. Swartz et al. (2011) N(ULX)/L(FIR)	2.0	3.8